Thermal Plume Transport from Sand and Gravel Pits – Potential Thermal Impacts on Cool Water Streams

Jeff M. Markle and Robert A. Schincariol
February 2007

Department of Earth Science, University of Western Ontario, 1151 Richmond Street, London, Ontario, Canada, N6A 5B7

Abstract

We investigated the potential thermal impacts from below-water-table aggregate extraction on a cool-water stream supporting Brook trout (*Salvelinus fontinalis*) and cool-water macroinvertebrates. We monitored thermal plumes emanating from an aggregate pit through an unconfined, glacial-outwash aquifer. Our objectives were to complete a detailed assessment to quantify the persistence of thermal plumes in the subsurface, and establish a framework for guiding these investigations as the growing demand for aggregate increases pressures to pursue extraction in ecologically sensitive areas. During a 10-year period, we measured ground and surface water temperatures in an outwash aquifer and cool-water stream, including two periods of intensive monitoring (22 months and 2.5 years) focusing on plume movement from one aggregate pit. We quantified the aquifer hydraulic conductivity *K* at the laboratory and field scale, and characterized the effective thermal conductivity λ at an unprecedented level of detail. The mean *K*'s from the multi-scale tests span two-orders of magnitude, 1.8×10^{-4} to 1.7×10^{-2} m s^{-1}, and are related to the test support volume. The saturated λ has a mean of 2.42 W m^{-1} K^{-1}, ranges from 2.14 to 2.69 W m^{-1} K^{-1}, and is correlated to stratigraphic units (gravel, sand, and till). The annual temperature amplitude in the pit is 10ºC above up gradient ground water, and our results show that alternating warm and cool plumes persist in the aquifer for 11 months and migrate up to 250 m down gradient. The observed plume velocity (1.2 m d^{-1}) lags the ground water velocity (2.8 m d^{-1}) due to thermal retardation. Furthermore, hydraulic conductivity is shown to vary with the scale of the test and ground water velocities estimated from pumping tests may overestimate thermal plume velocities. While we focused on plume migration, our results demonstrate that assessing impacts on the aquatic community requires an integrated, multi-disciplinary study. This work can guide such assessments.

Abbreviations: ags: above ground surface; asl: above sea-level; bgs: below ground surface; BHS: Bruggeman-Hanai-Sen; GPR: ground-penetrating radar; MOP: multiple-offset profile; PVC: polyvinyl chloride; XRD: X-ray diffraction; ZOP: zero-offset profile.

Introduction

Ground water discharge to streams and rivers exerts a fundamental influence on stream and river ecology (Elliott, 1994). The distribution of aquatic animals often reflects the timing and availability of ground water discharge volume, distribution, and temperature in order to fulfill various life cycle requirements. Areas of cool discharging ground water moderate stream temperatures by cooling the stream in the summer and warming the stream in the winter. Thus the diel and annual temperature fluctuations of the stream are subdued compared to air temperature. This provides areas of thermal refuge for aquatic animals and creates thermal conditions suitable for cool- and cold-water aquatic fauna. For example, many macroinvertebrates use the streambed substrate (the hyporheic zone) in areas of discharging ground water for critical development stages and as refuge from adverse conditions within the stream (Hynes, 1983; Pugsley and

Hynes, 1986). In particular, during the egg and pupal stages, these insects are not mobile and must tolerate the temperature conditions present within the streambed. Furthermore, aquatic insects do not acclimate generally, and some species have critical temperature thresholds above which acute mortality occurs (e.g., deKozlowski and Bunting, 1981; Quinn et al., 1994; Chadwick and Feminella, 2001). For some aquatic insects, there is evidence that increases in ambient winter stream temperatures result in early emergence, and diminished adult size and fecundity (Vannote and Sweeney, 1980; Hogg and Williams, 1996; Taylor and Dykstra, 2005). Reduced adult size affects reproduction potential and the competitive ability of the affected species within the aquatic community. As well, seasonal temperature patterns may be a critical factor in maintaining temporal segregation of competing macroinvertebrates and in determining the stability and number of species in a given community (Vannote and Sweeney, 1980). Moreover, temperature changes affecting one species within a macroinvertebrate community may have a positive or negative effect on other species within the community either directly or indirectly through complex interactions with processes involving energy cycling and organic matter dynamics (Lakly and MacAurthur, 2000; Nislow and Lowe, 2006). Such perturbations can affect the natural stream ecosystem, and these effects may even extend to the higher trophic levels such as fish.

Several studies have shown that the moderating influence of discharging ground water on the surface water temperature enhances the spawning and nursery habitat potential for several species of trout (e.g. Cunjak and Power, 1986; Curry et al., 1995; Acornley, 1999; Baxter and McPhail, 1999). Thus, in addition to indirectly affecting higher trophic levels, such as fish, changes to ground water and surface water temperatures may directly affect this group. In southern Ontario, Canada, native brook trout (*Salvelinus fontinalis*) spawn most commonly at stream temperatures between 6 and 8ºC between early October and mid- to late November (Witzel and MacCrimmon, 1983). The fertilized eggs are buried in the gravel and sand substrate of the stream where they incubate and hatch as free embryos (alevins) in midwinter. The alevins remain in the streambed substrate and emerge in late March to early May (Power, 1980). Successful incubation relies on stable temperature conditions with the optimum incubation temperature between 6 and 8°C (Marten, 1992), and with 50% mortality above 11.7°C (Hokanson et al., 1973). During the winter, the embryos are not mobile and must survive the thermal regime present in the hyporheic zone. During this period, ground water discharge keeps stream temperatures above 0°C, preventing anchor ice formation that would freeze the immobile embryos and alevins. Also, the water temperature greatly influences growth rates and development time decreases with increasing incubation temperatures (Garside, 1966). Early emergence, resulting from increased incubation temperatures, may increase exposure of fry to high-flow events, and alter the natural synchrony between emergence and the presence of a food supply (Noakes, 1989; Curry et al., 1995; Power et al., 1999). Thus, even small changes in the timing and temperature of discharging ground water can adversely affect temperature-sensitive species present in the discharge areas.

The link between the ground water and surface water interaction and the biotic system has recently become the topic of renewed interest as we move toward integrated watershed management (e.g. Hynes, 1983; Brunke and Gonser, 1997; Holmes, 2000; Hunt and Wilcox, 2003; Hunt et al., 2006). Several studies have shown that anthropogenic activities can alter ground water and surface water temperatures causing measurable changes to the biotic communities. For example, forestry operations have been shown to alter the temperature of discharging ground water changing the structure and density of both the macroinvertebrate and fish communities (e.g. Lynch and Rishel, 1984; Curry et al., 1995; Curry et al., 2002; Nislow and Lowe, 2006). Increases in discharging ground water temperature were shown to alter all levels of the aquatic community including both the plant and benthic invertebrate communities, as well as changing the rates of organic matter decomposition and thus energy cycling (Taylor and Dykstra, 2005). Andrews and Anderson (1979) investigated the influence of a 200-ha power plant cooling lake in Wisconsin on the ground water temperature. Their monitoring showed that the thermal disturbance to the ground water was limited to 100 m down gradient from the lake. There has been speculation that aggregate extraction may alter the temperature of ground water and nearby streams. Aggregate resources are commonly associated with glacial outwash deposits that also often support cool-water streams. The excavation of aggregate material below the water table involves removal of the forest cover and soil, followed by excavation of the unsaturated and saturated porous medium. The result is a pond, often hectares in area, where forest cover existed previously. The energy transfer across the air-water interface of the pond is many times larger than the energy transfer across the water table prior to extraction due to the removal of the vegetation and unsaturated zone. As a result, the temperature of the water in the pond is different from the pre-existing ground water. In summer months, the water in the pond is much warmer and in the winter it is colder. Since the water in these ponds is simply exposed ground water, it continues to move under the influence of the hydraulic gradient in the surrounding aquifer. Thus, the water moves back into the ground water system down gradient of the ponds and through the aquifer as a series of alternating warm and cool thermal plumes. If sufficient subsurface travel time (to enable equilibration to background temperatures) is not provided prior to discharge to the stream, altered stream temperature may result. When temperature changes are sufficient, adverse impacts on thermally sensitive fauna, such as macroinvertebrates and cold-water fish communities, will result. The increasing demand for aggregates has created pressure to extract aggregates in areas associated with sensitive cool-water streams and wetlands.

In this study, we measured the ground water temperature down gradient of an aggregate pit, during a 22-month period, using a dense network of monitoring wells. We quantified hydraulic properties of the glacial outwash aquifer at the laboratory and field scale, and characterized the aquifer thermal properties at a level of detail not previously reported in the literature. Our objectives were to measure thermal plume movement from an aggregate pit through an unconfined, sand and gravel aquifer, to quantify the distance across which thermal plumes persist in the subsurface under natural gradient conditions, and to establish a framework that researchers and practitioners may use to design

investigations integrating hydrogeology and stream ecology where the impacts from thermal disturbances to the ground water are of concern. Here we present a description of the field site, the investigation methods, the aquifer physical properties, the linkage between the ground water and surface water, and thermal plume migration observed along a two-dimensional section. In this study, we focused on the migration of the thermal plumes through the aquifer, and we did not attempt to measure specific impacts on the biotic community (macroinvertebrates and fish) in a nearby creek. Such an assessment will require a highly integrated, multi-disciplinary study that is beyond the scope of this study; however, this work can be used to design and plan such an assessment at this or other locations, and to better inform conservation decisions and management of developments involving aggregate extraction.

Description of Research Site

A multi-year study of thermal plume migration through an unconfined aquifer was completed in the Tricks Creek watershed. The Tricks Creek watershed is a small headwater system (26 km^2) located in southwestern Ontario, Canada, ~180 km west of Toronto (Fig. 1). Tricks Creek lies within a wetland complex that encompasses an area of ~105 ha (4% of watershed). The Tricks Creek wetland complex is a long, narrow, riverine type wetland. The headwaters for Tricks Creek originate in the northern portion of the wetland, flow to the south for approximately 4 km, and discharge into the Bayfield River (43°34′55.5″ N, 81°35′14″ W). Two small tributaries enter the creek, one from the west and one from the east. We have extended the watershed to include the small creek to the west as it discharges to the Bayfield River at the same point as Tricks Creek. In the upper reach, Tricks Creek is slow moving and meanders through the wetland. The streambed is predominantly silt with thick organic sediments in most locations. In the lower reach, the creek is fast moving with alternating riffles and pools. Here the streambed is dominated by sand and gravel substrate with small cobbles and boulders. The creek has an average streambed gradient of 0.002 m m^{-1}, and is generally small, ranging from 1 to 4 m in width, and from 0.25 to 1.5 m in depth. The mean annual flow is 0.45 m^3 s^{-1}, with peak flows of 2.3 m^3 s^{-1}. Under baseflow conditions (July to September), the average flow of 0.3 m^3 s^{-1} is maintained entirely from ground water discharge from the glacial outwash. Tricks Creek is characterized by cool water with a mean annual temperature of 12.9°C. The maximum average daily water temperature is 22.2°C (July to August), and the minimum average daily water temperature is 3.2°C (February). These stream temperatures support resident brook and rainbow trout (*Salmo Gairdneri*) populations, and a diverse assemblage of macroinvertebrates, typical of a cool, headwater stream. Benthic invertebrate sampling at one location on Tricks Creek found between 23 and 37 different taxa comprising Ephemeroptera (mayflies), Plecoptera (stoneflies), Trichoptera (caddisflies), and Diptera (R. Griffiths, *unpublished data*). In order of abundance were Ephemeroptera (main taxa included epemerellidae, baetidae and leptophlebiidae mayflies), Diptera (main taxa included chironominae tanypodinae, and tipulidae), Plecoptera (main taxa included chloroperlidae, leuctridae and perlodidae stoneflies), and Trichoptera (main taxa included goeridae, hydropsychidae, lepidostomatidae and philopotamidae caddisflies).

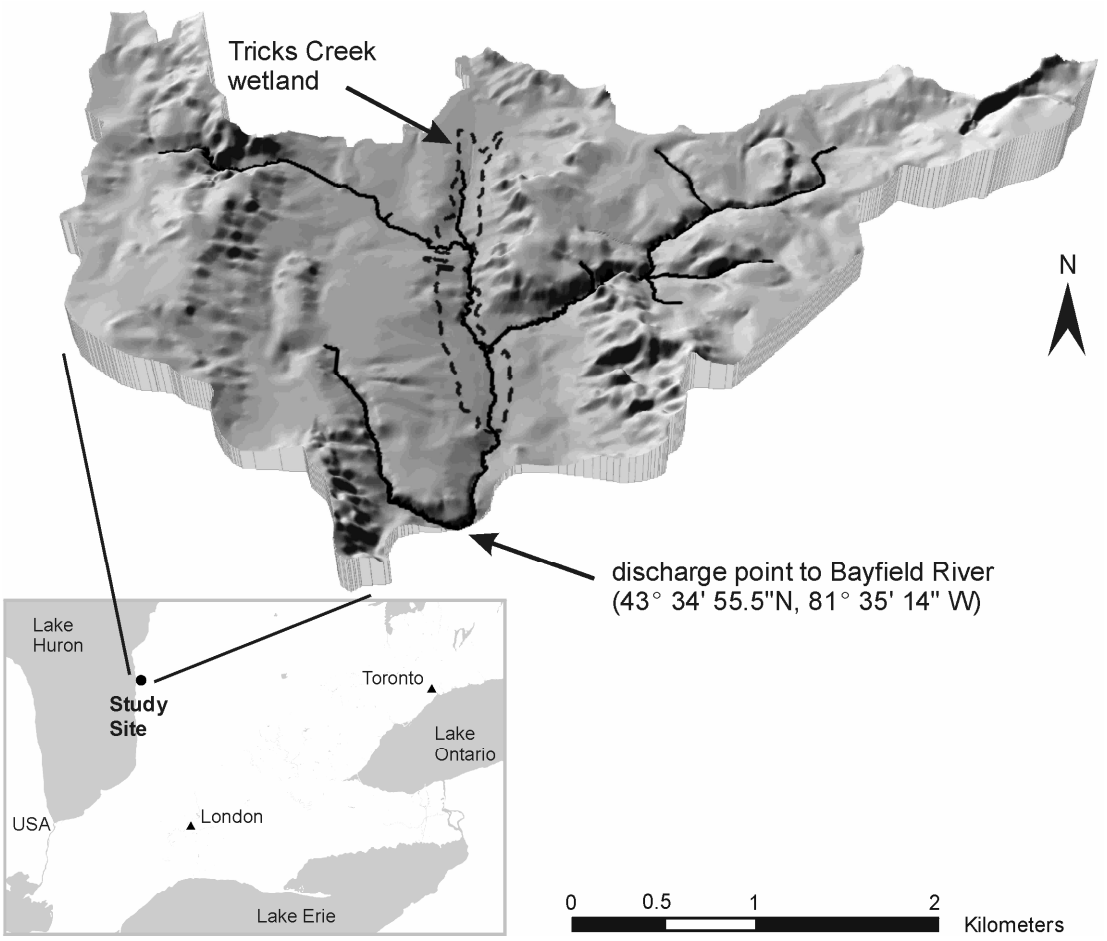

Figure 1 Study area location map and three-dimensional view of the Tricks Creek watershed and wetland.

The topography of the watershed is characterized by a broad north–south trending valley that slopes from an elevation of 260 m asl (above sea-level) at the northern boundary to 245.8 m asl at the southern point where the creek discharges to the Bayfield River. The valley is bounded on the east and west by gently rising hills which reach maximum elevations of 300 m asl on the east and 285 m asl on the west. Climatic records for the Goderich, Ontario weather station (43°46′ N, 81°43′ W), 19 km to the northwest, and the Blyth, Ontario weather station (43°43′ N, 81°22′ W), 15 km to the northeast, indicate the mean monthly temperature from 1971–2000 varied from a low of –7.5ºC in January to a high of 20.2ºC in July. The average annual temperature is 6.8ºC and the mean annual precipitation is 1184.3 mm yr^{-1}, with 350.4 cm as snow (Environment Canada, 2005).

Tricks Creek and the surrounding wetland complex lie on the eastern edge of a former glacial outwash channel that trends north–south. The outwash deposits are laterally confined to the west by the Wyoming Moraine and to the east by the Wawanosh Moraine, and unconformably overlie the contact between these moraines (Fig. 2a). Formed 13,000 years before present during the Port Huron Stadial of the Wisconsinan glaciation, the outwash was deposited in a meltwater channel that was cut into the underlying sediments during the last glacial retreat, (Cooper and Fitzgerald, 1977; Barnett, 1992). The outwash is composed of poorly-sorted to well-sorted sandy gravel to gravely sand with cobbles, boulders, and traces of silt. It is mainly gravel and sand in the northern portion of the valley becoming progressively finer to the south where it is mainly fine to medium sand. The meltwater channel scoured into the tills most deeply along the western edge of the channel, depositing between 20 and 30 m of outwash material along this edge in the northern portion of the watershed and 10–15 m in the south. To the east, the channel was much shallower with approximately 5–10 m of sand and gravel beneath Tricks Creek (Fig. 2b). The glaciofluvial outwash deposit represents a significant aggregate resource, and several sand and gravel extraction operations are active along the western edge of the wetland.

Glacial moraine deposits are present across the entire study area. The Wyoming Moraine consists of variable loose stony silt till. The Wawanosh Moraine consists primarily of ice contact stratified drift deposits, and some occurrences of silt to sandy silt till along the western margin of the moraine (Cooper and Fitzgerald, 1977). Within the watershed, the moraine deposits vary in thickness from approximately 25 to 45 m. The moraine deposits sit unconformably on top of the truncated surface of the Middle Devonian Dundee Formation. Generally, the Dundee is a grey brownish grey, medium- to fine-grained, fossiliferous limestone and dolomitic limestone (Liberty and Bolton,

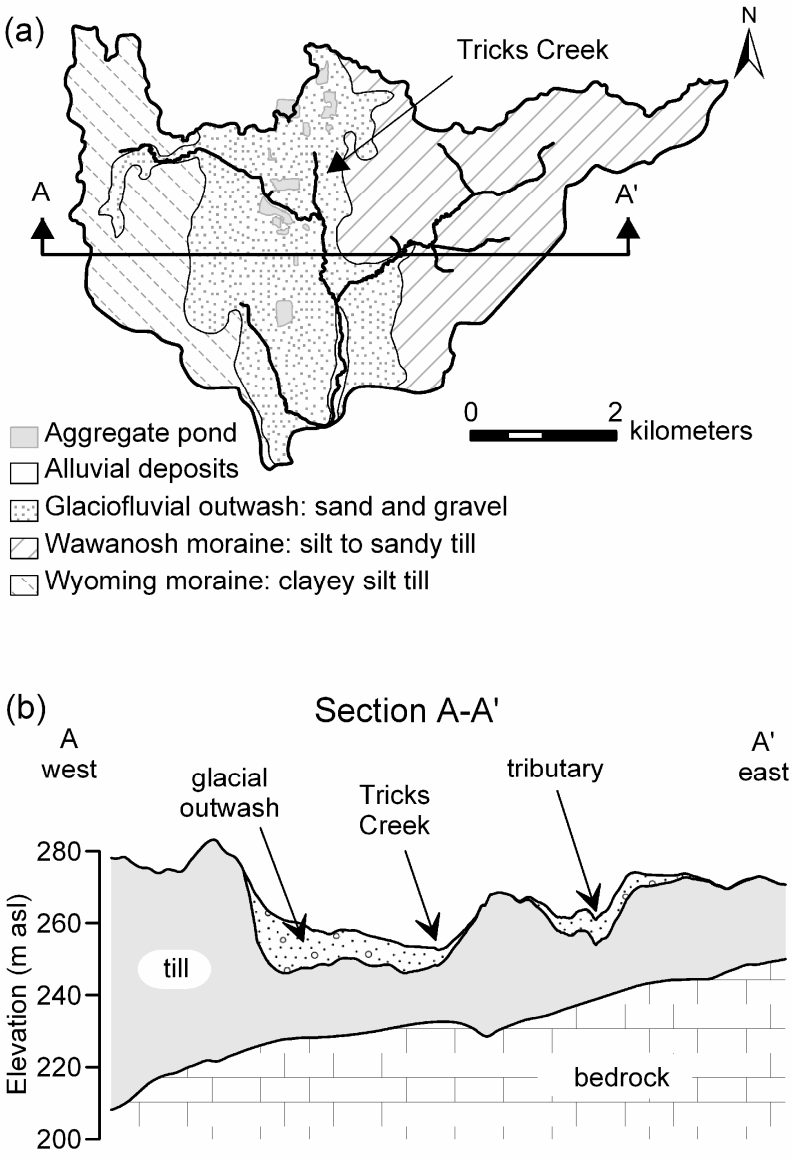

Figure 2 Quaternary geology for the Tricks Creek watershed (Fig. 2a, adapted from Cooper and Fitzgerald, 1977) and a geological cross-section (Fig. 2b).

1971). Within the Tricks Creek catchment area, the bedrock surface slopes gently in a westerly direction (0.006 m m^{-1}).

The glacial outwash forms an unconfined sand and gravel aquifer. The depth to the water table ranges between 0.2 and 4 m bgs (below ground surface). The regional ground water flow direction within the catchment is from north to south where ground water discharges to the Bayfield River (Fig. 3). The water table elevation at the top of the catchment is approximately 255.5 m asl, dropping to 244 m asl at the southern end of the catchment. In the north portion of the catchment, the horizontal hydraulic gradients are very low (<0.001 m m^{-1}). Near Tricks Creek the gradients increase significantly and ground water flows toward the creek. At the southern end of the catchment, the influence of the Bayfield River increases the horizontal gradient (>0.005 m m^{-1}). The unconfined aquifer is bounded laterally and from below by a till aquitard. To the north, the aquifer is bounded by a ground water and surface water divide. The water table aquifer is recharged only by precipitation that falls within the catchment, and all the ground water eventually discharges to Tricks Creek or the Bayfield River.

In this study, we observed thermal plume migration down gradient of an existing aggregate operation. The site is located approximately 1/3 of the way down the catchment (Fig. 3). The sand and gravel extraction proceeds by first clearing the forest cover and removing the soil and porous medium above the water table, and then excavating the porous medium below the water table. The pond, created by the extraction operation, covers approximately 5 ha and varies between 4 and 6 m in depth. The pond is about 50 m west of the wetland and 100 m west of Tricks Creek. The regional potentiometric surface shows that the ground water flow path from the pond to Tricks Creek is ~750 m in length. The western tributary of Tricks Creek crosses this flow path about 400 m down gradient of the pit. The horizontal hydraulic gradient in the area of the pit is between 0.001 and 0.004 m m^{-1}.

Temperature measurements made in the monitoring wells shown in Figure 3 demonstrate that the annual range of ground water temperature in the outwash decreases with depth. At a depth of 3 m bgs, temperatures range from an average maximum of 12.7ºC (September) to an average minimum of 5.0ºC (March), with a mean annual temperature of 9.2ºC. This annual variation of approximately 7ºC is the combined result of heat transport from the ground surface by conduction as well as by convection with water infiltrating through the unsaturated zone and into the saturated porous medium. From measurements at a series of streambed piezometers, we determined the mean annual temperature of ground water discharging to Tricks Creek to be approximately 10.3ºC.

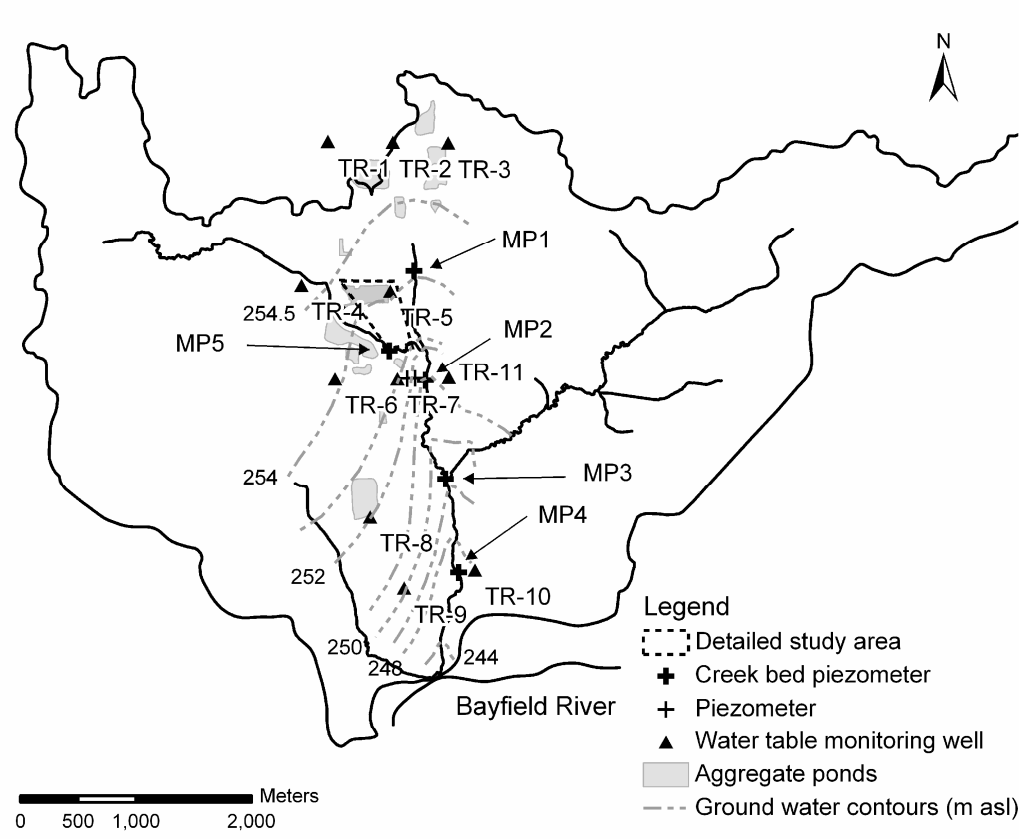

Figure 3 Monitoring well locations and potentiometric surface in the glacial-outwash sand and gravel aquifer. The location of the detailed study area is shown by the dashed polygon.

Materials and Methods

Twenty-nine monitoring wells were installed in two phases during the course of this study. In phase one, 17 wells (M0–M16) were installed and temperatures were monitored for a 22-month period (Fig. 4a). During this period only a limited amount of aggregate extraction occurred. Subsequent aggregate extraction resulted in the removal, or destruction, of the first 35 m of the monitoring well network (eight wells) as the down-gradient pit face advanced south. Extraction ceased again and we installed 12 additional wells (M17–M28) for the purposes of a large-scale aquifer test and a cross-hole GPR (ground-penetrating radar) survey (Fig. 4b).

Monitoring network and instrumentation

In phase one, 15 multilevel piezometers and two water table monitoring wells (M8 and M15) were installed in February 1995 (Fig. 4a). We installed the majority of the wells within the first 150 m down gradient of the pond based on preliminary modeling results (Yang, 1995). The most distant well was 325 m down gradient. Well TR-5, along the east side of the pit, is a water table well installed in a preliminary investigation. Each

multilevel piezometer consisted of 0.0095-m outside diameter (OD) polyethylene tubes bundled to a 0.025-m-diameter PVC (polyvinyl chloride) pipe. A 0.10-m section of each polyethylene tube was perforated and covered with nylon screen. In most cases, a 0.3–0.6-m section of the PVC pipe was also screened. These wells provide measurements at discrete points vertically within the aquifer. The water table monitoring wells were constructed with 0.05-m diameter, schedule 40 PVC pipe, and each well was screened across the aquifer with a 6.1-m long, 20 slot PVC screen. The abundance of cobbles precluded sample collection and we determined the stratigraphy based on observations during drilling.

We installed 12 additional monitoring wells in a second phase of drilling in January 2001 for use in a large-scale aquifer test and a GPR survey (Fig. 4b). These wells included eight multilevel wells, three water table wells (M17, M19, and M21), and one pumping well (M26). The pumping well was completed as a 0.2-m diameter, schedule 40 well with a 3-m long, 50 slot PVC screen. The well was backfilled with No. 3 sand up to 1 m above the well screen and natural collapse material above. For this phase of the drilling, the auger rig was equipped with a 1.8-m-long continuous soil sampler that facilitated the collection of relatively undisturbed soil cores with a 0.127-m diameter. Core recovery rates with this method were approximately 50%.

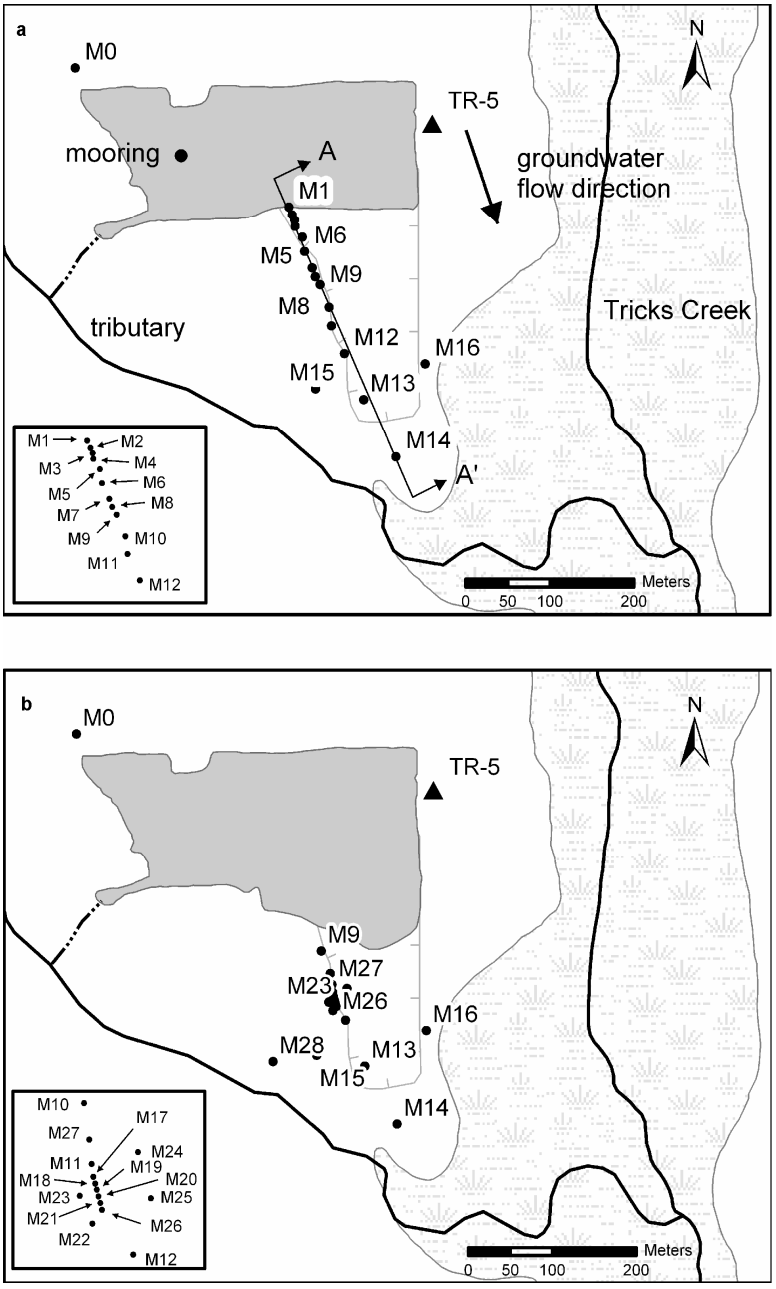

Figure 4 Detailed study area and monitoring well location map. The initial pit configuration and monitoring well network in the first phase of the study is shown at the top (Fig. 4a). The pit configuration and monitoring well network during the second phase of the study is shown at the bottom (Fig. 4b) and the inset shows in detail the well locations.

We monitored ground water levels periodically at the array of piezometers. During the initial 22-month monitoring period, water levels were monitored continuously in the pond and at wells, M8 and M13, by data loggers with Druck pressure transducers. Ground water temperature measurements were taken at an array of 128 thermistors installed in the wells (M0–M14) and connected to a series of Campbell Scientific, CR10 data loggers. The accuracy of the thermistors across the observed temperature range was ±0.2°C. Ground water temperatures were recorded from July 1995 to May 1997 for wells M0–M14. In May 1997, the instrumentation in wells M1–M9 was removed due to the advance of the pit face. Monitoring continued at the remaining locations until December 1997. Monthly ground water temperatures were collected manually at M15 and M16. Soil heat flux was monitored with two soil heat flux plates (HFT-3 Heat Flow Transducer manufactured by Radiation and Energy Balance Systems) installed 0.05 m BGS. One plate was located at M12 and the other was located at M14. Near surface atmospheric conditions were monitored near M14. Air temperature was monitored at heights of 1 and 2 m ags (above ground surface) with two Campbell Scientific 207 Temperature probes. Precipitation was recorded with a Geneq P-1000 tipping-bucket rain gauge during the spring, summer, and fall. During the winter, the snow depth was measured with a Campbell Scientific UDG01 Ultrasonic Depth Gauge from which an equivalent rainfall was estimated. Data loggers measured the sensors every 30 s and stored average values every 30 min.

We established a mooring in the pond at which we measured surface water temperature at four elevations for a 51-month period, from June 1993 to August 1997 (Fig. 4). Three submersible Brankner temperature data loggers monitored the temperature at 0.35 m, 2.4 m and 4.5 m above the pond bottom. The water temperature near the pond surface was monitored by a thermistor floated 0.05 m below the water surface. The average annual depth of the pond at the mooring was 6 m.

We installed mini piezometers in the creek bed at five locations (MP1–MP5) during the course of the study (Fig. 3). At each location, three piezometers were driven to depths ranging between 0.35 and 1.8 m below the streambed. We manually measured both surface water and ground water levels and temperatures at these locations with two exceptions. At MP4 and MP5 water levels and temperatures were measured with a combination of electronic and manual methods. Two of these monitoring locations (MP2 and MP4) are brook trout redds (spawning and nursery sites). At the remaining sites the streambed substrates are fine grained making them unsuitable spawning locations. However, we monitored temperatures and water levels at these locations to observe the ground water – surface water interactions at locations distributed along the creek.

Aquifer physical properties

Glacial outwash deposits are heterogeneous deposits, having large variations in hydraulic conductivity (e.g. Hess et al., 1992; Rehfeldt et al., 1992; Anderson et al., 1999; Oldenborger et al., 2003). Properly characterizing these spatial variations in hydraulic

conductivity, at a scale appropriate for the field problem under investigation, is critical for understanding the movement of fluid and heat through the porous medium. To this end, we completed a multi-scale assessment of the hydraulic conductivity using a variety of direct and indirect methods. These included grain-size analysis and constant-head permeameter tests on the soil cores in the laboratory, falling-head tests in the monitoring wells, a cross-hole GPR survey, and a two-day constant discharge pumping test. We completed constant-head permeameter tests on 32 soil cores obtained from nine boreholes. The permeameter design allowed multiple values of hydraulic conductivity to be determined along the length of the core (Boggs et al., 1990; Wolf et al., 1991) and we obtained estimates of permeability for 160 subsections of the core with a mean length of 0.1 m. For each core, we applied five or more different head drops across the permeameter and measured the flow rate. The estimated permeability was determined from the average of these tests. Viscosity and density corrections were applied, and hydraulic conductivities are reported at 10°C.

After permeameter testing was completed, we sectioned the cores from M17 and M19 at each pressure measurement point, and completed grain-size analysis and determined the porosity for each subsection. Estimates of the permeability were obtained with the empirical relation of Kozeny–Carman (Kozeny, 1927; Carman, 1937, 1956) given as

$$K = \left(\frac{\rho_w g}{\mu_w} \right) \frac{\phi^3}{C S_S^2 (1-\phi)^2}, \qquad [1]$$

where C is a factor accounting for the tortuosity of the pore spaces, g is the gravitational acceleration, ρ_w is the density of water, μ_w is the dynamic viscosity of water, and S_S is the specific surface area of the soil particles per unit volume of particles. Carman (1956) reported the value of C to be 4.8 ± 0.3 for uniform spheres, and C is generally taken to be 5. The specific surface area may be estimated from the particle size distribution curves (Carrier, 2003). We selected the Kozeny–Carman formula as it provides direct estimates of K with porosities obtained from both the GPR survey and the soil cores, and it is preferred over other common relations such as Hazen (Carrier, 2003).

We conducted falling-head tests in 75 piezometers in the multilevel wells and eight water table wells, and determined the aquifer hydraulic conductivity by methods for high conductivity formations (Butler, 1997). A minimum of three tests, with different initial heads, were completed in each piezometer and the hydraulic conductivity was estimated from the average of the measured values.

The average hydraulic properties of the aquifer were obtained from an aquifer pump test. We conducted the test at a constant pumping rate of 0.0228 $m^3 s^{-1}$ for a period of 48 h. Discharge was measured by a flow rate meter and totalizer. During the test, we measured water levels with a water level meter in 35 piezometers (14 multilevel wells),

four water table monitoring wells, and six 0.025-m-diameter PVC piezometers. In addition, drawdown data were measured in the pumping well and nine piezometers with pressure transducers connected to data loggers. All the observation wells were within a 155-m radius of the pumping well. We applied Moench's (1997) method of analysis for pumping tests in anisotropic, unconfined aquifers to the data to obtain estimates of aquifer hydraulic properties.

We collected GPR tomographic data across six boreholes (M17–M21, and M26), which span a 12.3-m-wide by 7.6-m-thick portion of the aquifer, with a Sensors and Software (Mississauga, ON) pulseEKKO 100 GPR system equipped with borehole antennas (Fig. 4b). We completed surveys using two different antenna configurations. For the first configuration, ZOP (zero-offset profile), we moved the transmitter and receiver antennas down their respective boreholes in unison. For the second configuration, MOP (multiple-offset profile), we held the receiving antenna fixed and moved the transmitting antenna down the borehole until it had occupied all possible positions. Then the receiver was moved and the process repeated until both antennas had occupied all possible positions. We completed five ZOP surveys using 100 MHz antennas and a pulser voltage of 400 V. The borehole separation ranged from 4.85 to 13.53 m, and the profiles began at the ground surface and proceeded to the bottom of the borehole with a step size of 0.125 m. Six MOPs were completed with 200 MHz antennas and a pulser voltage of 400 V. The borehole separation ranged from 2.35 to 6.92 m. For the MOPs we collected the first trace just below the water table and the final trace at the bottom of the borehole with a step size of 0.25 m.

We inverted the travel times to reconstruct the horizontal and vertical structure with Pronto (Aldridge and Oldenburg, 1993), a curved-ray tracing tomographic inversion code. The inversions were performed with the domain divided into 0.25-m square cells. The porosity for each cell block was estimated from the inverted slowness field with the BHS (Bruggeman–Hanai–Sen) mixing formula (Sen et al., 1981; Feng and Sen, 1985) given by

$$\phi = \frac{\left(\varepsilon_{eff} - \varepsilon_s\right)}{\left(\varepsilon_{wa} - \varepsilon_s\right)} \left(\frac{\varepsilon_{wa}}{\varepsilon_{eff}} \right)^C , \qquad [2]$$

where ε_{wa} and ε_s are the dielectric constants of water and air respectively, ε_{eff} is the measured dielectric constant of the saturated soil, and C is a shape factor (1/3 for spherical grains). Using the GPR-determined porosities and the Kozeny–Carman equation (Eq. [1]), we estimated the aquifer hydraulic conductivity.

In addition to GPR-determined porosity, measurements of aquifer porosity, as well as bulk density and soil particle density were made for 31 subsections of soil cores obtained from boreholes M17 and M19. The bulk density was estimated from the measured dimensions and dry mass of the core segments. The sample porosity was taken

to be the average of the porosity estimated from the difference in mass between saturated and oven dried samples, and the porosity estimated from the measured sample volume and mean grain density.

The heat capacity of the aquifer solids C_s can be determined from the known mineral composition using

$$C_s = \sum_{i=1}^{N} f_i \left(c_s \rho_s\right)_i \ , \qquad [3]$$

where N is the number of mineral phases, f_i is the volume fraction of the mineral phase i, and c_s and ρ_s are the specific heat and density of each mineral phase, respectively. The heat capacity of a variably saturated porous medium C_0 can be determined by

$$C_0 = (1-S)\phi c_a \rho_a + S\phi c_w \rho_w + (1-\phi)C_s \, , \qquad [4]$$

where S is the saturation level, c_a and ρ_a are the specific heat and density of air, and c_w and ρ_w are the specific heat and density of water. For temperatures ranging from 0 to 50ºC, the heat capacity of the air phase is negligible relative to the water and solids (Luckner and Schestakow, 1991), and the first term of Eq. [4] is generally ignored.

We measured the thermal conductivity of the aquifer solids λ_s in the laboratory on 41 samples using the divided-bar apparatus (Sass et al., 1971). On a subset of 27 samples, we determined the mineralogy by XRD (X-ray diffraction) techniques. From the known mineral compositions, we estimated the bulk thermal conductivity for the aquifer solids λ_s, having n mineral components with a volume fraction x_i and conductivity λ_i, using the geometric mean equation given by

$$\lambda_s = \prod_{i=1}^{n} \left(\lambda_i^{\,x_i}\right). \qquad [5]$$

Results and Discussion

Figure 5 is a geological cross-section from the pit south along the monitoring well network. The ground surface elevation varies along the section as the result of the extraction activity. In the first 50 m down gradient of the pond, most of the unsaturated sand and gravel have been excavated, and the top soil has been removed in area up to 290 m down gradient of the pond. As well, between 200 and 290 m, the unsaturated sand and gravel has been removed (Fig. 4a and Fig. 5). Surface extraction has not proceeded beyond 300 m down gradient of the pond edge. Along the section, approximately 6 m of gravel and sand overlie the till. The majority of the material is undifferentiated gravel and sand with boulders and cobbles. A 1- to 2-m-thick layer of medium to coarse sand overlies the till along a portion of the section with the occasional lense of medium to

coarse sand found within the gravel. From the grain-size analyses, the material ranges from poorly-sorted to well-sorted gravel and sand with little or no fines (generally <5% silt). Over 65% of the material recovered was gravel with the remaining being fine to coarse sand. The geometric mean particle diameter (Shiozawa and Campbell, 1991), d_g, for the gravel ranges from 4.3 to 19.0 mm with an average value of 11.3 mm. For the sand, d_g ranges from 0.3 to 8.9 mm with an average value of 4.2 mm. The mineral composition of the 27 outwash samples (Table 1) is primarily calcite, dolomite, quartz, and plagioclase feldspar (Markle et al., 2006). Some samples contain hornblende, illite, montmorillonite, and chlorite or possibly kaolinite in minor quantities (<5% total).

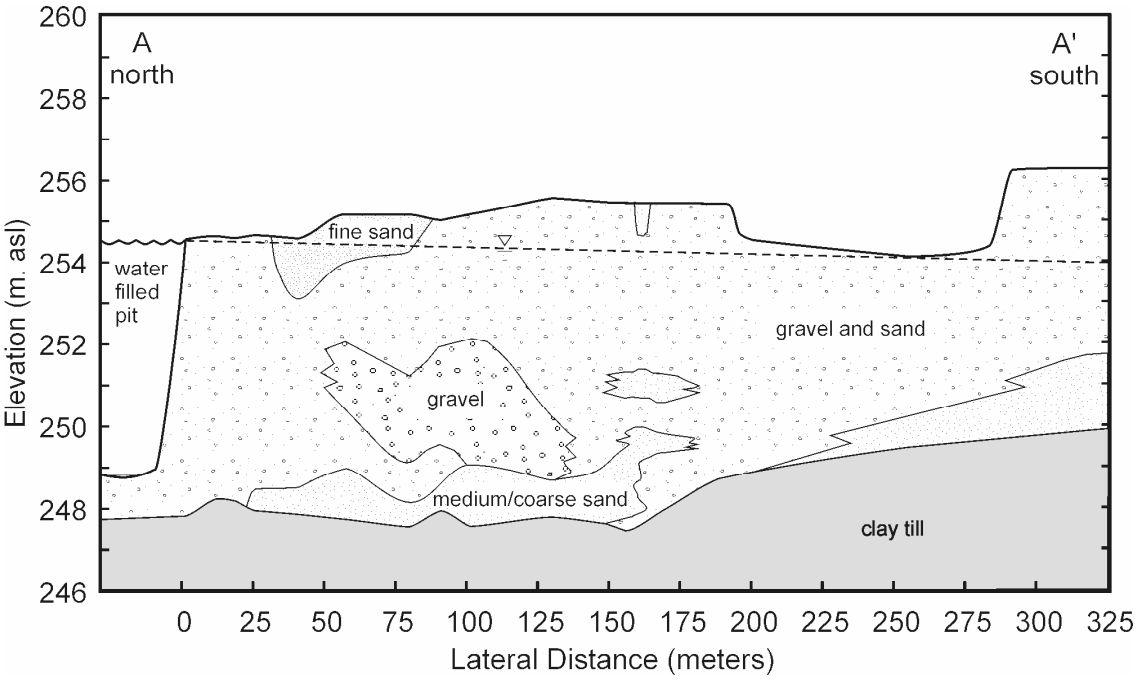

Figure 5 Geologic cross-section A–A' through the outwash deposit.

Table 1. Average mineral composition determined by X-ray diffraction and calculated using the integrated peak area method.

	Mineralogical composition (average volumetric fraction†)		
Mineral	Gravel, $n = 6$	Fine to coarse sand, $n = 17$	Till, $n = 3$
Calcite	0.44 ± 0.07	0.29 ± 0.04	0.32 ± 0.04
Dolomite	0.36 ± 0.05	0.36 ± 0.04	0.40 ± 0.09
Anorthite	0.02 ± 0.04	0.08 ± 0.04	0.04 ± 0.03
Hornblende	0.006 ± 0.005	0.006 ± 0.002	0.003 ± 0.003
Quartz	0.17 ± 0.04	0.25 ± 0.06	0.22 ± 0.07
Illite	0.005‡	0.003	0.009 ± 0.006
Montmorillonite		0.004 ± 0.002	
Chlorite/kaolinite	0.0014 ± 0.002	0.001 ± 0.001	0.0032 ± 0.003

One sample from the soil horizon contained a large fraction of organic material and was not included in this table.

† Reported values are average volumetric fractions ± 95% confidence interval.

‡ A confidence interval could not be calculated where <3 samples contained this mineral.

The porosity of the aquifer ranges from 0.18 to 0.39 (Table 2). GPR-determined porosities compare well with porosities measured on the aquifer cores. The mean and standard deviation of the GPR-determined porosities were 0.294 ± 0.002 and 0.031 m^3 m^{-3}, respectively, and the mean and standard deviation of the core-determined porosities were 0.274 ± 0.022 and 0.057 m^3 m^{-3}, respectively. The mean porosity from the core segments is 7% lower than that determined from the GPR. This difference may be due to consolidation during core extraction (Wolf et al., 1991) or under representation of higher porosity layers in the recovered core. Therefore, we assume a porosity of 0.29. We found the porosity was not correlated to stratigraphic units, but rather it varied with depth. We believe the variation may be related to small changes in the depositional environment which occurred as the vertical sequence of aquifer material was deposited. The mean bulk density of the 29 cores was 1.92 ± 0.058 g cm^{-3}, and the standard deviation of the measurements was 0.160 g cm^{-3}. The mean and standard deviation of the particle density measurements were 2.64 ± 0.033 g cm^{-3} and 0.090 g cm^{-3}, respectively.

Table 2. Statistical summary of aquifer porosity, bulk density, and particle density measurements.

Data source	Number of values *n*	Porosity ϕ		Bulk density ρ_b		Specific gravity	
		Mean ± C.I.†	*SD*‡	Mean ± C.I.	*SD*	Mean ± C.I.	*SD*
		——— m^3 m^{-3} ———		——— kg m^{-3} ———			
Core sections	29	0.274 ± 0.022	0.057	1.92 ± 0.058	0.160	2.64 ± 0.033	0.090
GPR	1164	0.294 ± 0.002	0.031				

† 95% confidence interval
‡ Standard deviation

Aquifer hydraulic properties

Estimates of hydraulic conductivity for the outwash sand and gravel range from 10^{-5} to 2.7×10^{-2} m s^{-1} (Table 3). The hydraulic conductivity for the till ranges from 10^{-9} to 10^{-11} m s^{-1} based on field-based falling-head tests. For the outwash, the hydraulic conductivity values are lognormally distributed (Fig. 6), and the geometric mean hydraulic conductivity, determined by permeameter and grain-size analyses, agrees well with values measured in the field by falling-head tests and cross-hole GPR with the MOP configuration (Table 3). We used Student's t-test to compare the mean hydraulic conductivities for the gravel and the sand, obtained by permeameter, grain size, and GPR. No significant difference ($\alpha = 0.05$) between the mean hydraulic conductivities was found. The horizontal hydraulic conductivity determined by GPR with the ZOP configuration was 1.5×10^{-3} m s^{-1}, and the horizontal hydraulic conductivity estimated from the constant discharge test was 1.7×10^{-2} m s^{-1}. The ratio of horizontal to vertical hydraulic conductivity determined from the pumping test was 5:1, which is within the range of anisotropy ratios reported for other sand and gravel aquifers: 7:1 to 17:1 for an alluvial terrace deposit (Boggs et al., 1990); 2:1 to 5:1 for glacial outwash (Hess et al., 1991), and 1.6:1 for glacial outwash (Moench, 2004). The variation in hydraulic

Table 3. Hydraulic conductivity *K* of the outwash sand and gravel at 10°C.

Test Method	Number of values *n*	Geometric mean hydraulic conductivity *K*	Variance ln(*K*)	Minimum	Maximum	Estimated support volume *V*
		m s^{-1}				m^3
Grain size†	60	5.2×10^{-4}	0.858	4.9×10^{-5}	5.0×10^{-3}	1.24×10^{-3}
Permeameter‡	158	4.1×10^{-4}	1.927	1.0×10^{-5}	2.7×10^{-2}	1.24×10^{-3}
Falling-head test§	75	1.8×10^{-4}	0.127	1.6×10^{-5}	2.9×10^{-4}	9.8×10^{-4}
Falling-head test¶	8	9.1×10^{-4}	1.551	1.9×10^{-4}	9.0×10^{-3}	7.0×10^{-3}
Ground-penetrating radar, MOP#	1249	6.0×10^{-4}	0.287	1.7×10^{-4}	2.1×10^{-3}	1.2
Ground-penetrating radar, ZOP††	169	1.5×10^{-3}	0.202	5.7×10^{-4}	4.0×10^{-3}	17.8
Heat plume	1	7.8×10^{-3}‡‡				4.0×10^{2}§§
2-day pumping test	1	1.7×10^{-2}				1.36×10^{4}

† *K* was estimated using the Kozeny–Carman empirical equation.
‡ The estimated *K* is representative of the vertical hydraulic conductivity.
§ Tests completed in 0.0095-m-diameter piezometers.
¶ Tests completed in 0.05-m-diameters wells.
# *K* estimated from the MOP (multiple-offset-profiles) for 0.25-m square cells using the Kozeny–Carman empirical equation.
†† *K* estimated from the ZOP (zero-offset-profiles) using the Kozeny–Carman empirical equation.
‡‡ *K* estimated from cross-correlation of the observed thermal plumes, with a porosity of 0.29 and hydraulic gradient of 0.0012.
§§ Support volume estimated by the length of aquifer considered in the cross-correlation analysis, the average thickness of the saturated zone of 5.5 m, and a 1-m-wide section of aquifer.

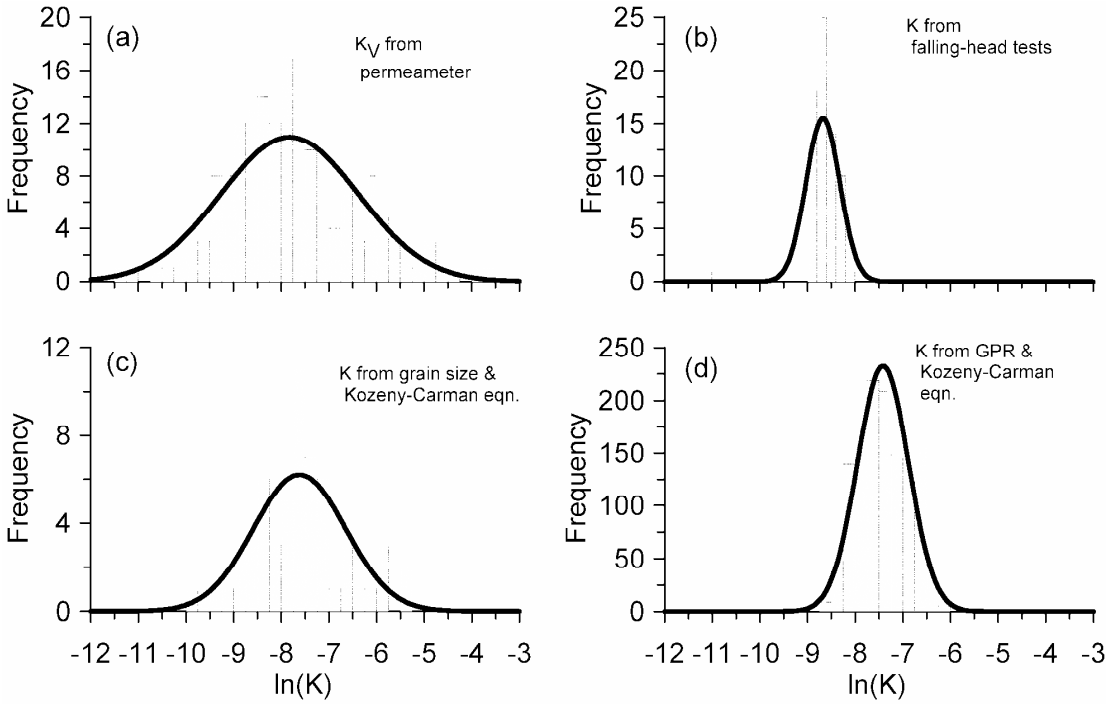

Figure 6 Distribution of ln(K) with the normal distribution curve shown by the thick line: (a) measured with the constant-head permeameter; (b) measured by in situ falling-head tests, and estimated from (c) grain-size analyses and (d) cross-hole ground-penetrating radar using the Kozeny–Carman equation.

conductivity with depth is shown in Figure 7. The vertical hydraulic conductivity, measured by the permeameter, varies across two-orders of magnitude (Fig. 7a) while estimates from grain-size analysis, which are isotropic values, vary across one-order of magnitude (Fig. 7b). Both profiles show that the hydraulic conductivity increases with depth. Also, the GPR-determined hydraulic conductivities show a step increase at a depth of 4.5 m, but have significantly less variation than the permeameter or grain-size values.

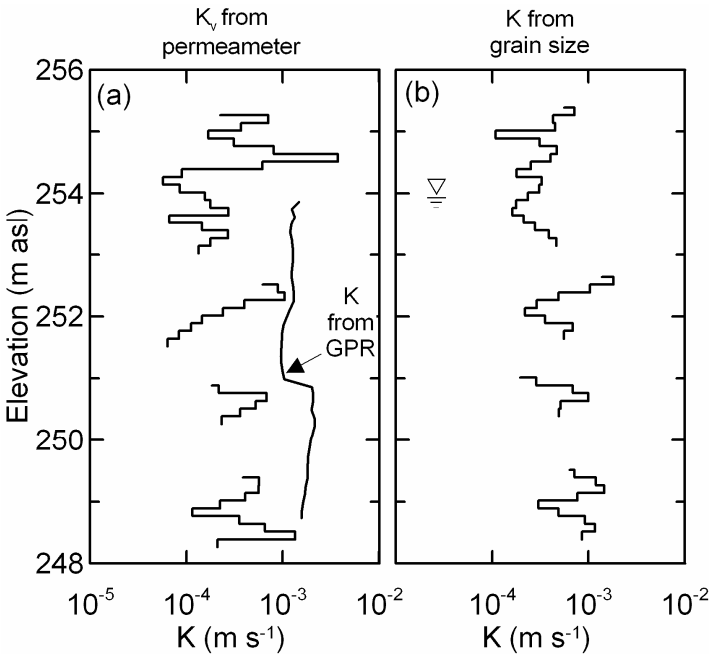

Figure 7 Vertical profiles of hydraulic conductivity K at 10°C. (a) K_v measured by permeameter. Values of K, estimated from the ground-penetrating radar (GPR) using the Kozeny–Carman empirical equation, are from a zero-offset profile completed between M17 and M19. These are representative of an average of the porous medium between the two wells. (b) K estimated from grain size using the Kozeny–Carman equation. These are depth-averaged values from the cores for wells M17 and M19.

These hydraulic conductivity values illustrate the effect of measurement scale. The mean hydraulic conductivity increases as the volumetric scale (support volume) of the test increases. The hydraulic conductivity from the 2-day pumping test is approximately two-orders of magnitude higher than values from most of the other tests. Similar differences between laboratory- and field-measured hydraulic conductivities have been reported for other glacial outwash aquifers. For example, Bradbury and Muldoon (1990) and Rehfeldt et al. (1992) reported differences of one- to two-orders of magnitude, and Wolf et al. (1991) and Rovey and Niemann (2001) reported differences of one-order of magnitude. These differences result, in part, from the volume of aquifer influenced during the test and how the heterogeneities encountered within this volume are spatially averaged by the test (e.g. Desbarats, 1994; Sánchez-Vila et al., 1996; Rovey and

Niemann, 2001; Beckie and Harvey, 2002; Molz et al., 2005). To investigate the dependency of our measured hydraulic conductivities on the measurement scale, we chose the test volume as a measure of scale (Bradbury and Muldoon, 1990; Schulze-Makush et al., 1999). Permeameter and grain size measurements were made on sections of core with an average test volume of 1.24×10^{-3} m^3 (~0.1-m-long by 0.125-m-diameter). We estimated the support volumes for the falling-head test and pumping test by calculating the volume of porous media required to accommodate or supply the volume of fluid injected or removed, during the test (Schulze-Makush et al., 1999). While we recognize that this method is an approximation of the volume of aquifer influenced by these two tests, it is simple to implement and provides a basis for comparing results. Methods that are more rigorous for estimating support volumes for pumping and slug tests have been developed for specific flow conditions (e.g. Desbarats, 1994; Beckie, 2001; Beckie and Harvey, 2002; Molz et al., 2005). However, applying these methods to the test conditions present at our site is outside of the scope of this research.

The GPR support volume can be approximated by the volume of the first Fresnel zone (Williamson, 1991; Červený and Soares, 1992; Reynolds, 2000). For a homogeneous medium, the Fresnel volume V depends on the path lengths of the ray trace L and the wavelength of the radar signal γ and is given by (Huisman et al., 2003)

$$V = \frac{4}{3}\pi abc\,, \qquad [6]$$

where a, b, and c are the semi-axes of the ellipsoid defined as

$$a = \frac{1}{2}\left(\frac{\gamma}{2} + L\right), \qquad [7]$$

$$b, c = \frac{1}{2}\left(\frac{\gamma^2}{4} + L\gamma\right)^{1/2}. \qquad [8]$$

The wavelength γ can be calculated from the load frequency of the transmitter GPR pulse f_L and the velocity in the medium separating the transmitter and receiver as v/f_L. The Fresnel zone is a circular region formed by the cross-section of the Fresnel volume in a plane perpendicular to the ray path. The maximum diameter of the Fresnel zone along the ray path is given by $2b$ and is considered to be the spatial resolution in tomography. Given the measured load frequency (45–50 MHz for ZOPs and 90–110 MHz for MOPs) and the survey geometry, the average Fresnel volume for the 100 MHz antennas was 17.8 m^3 (Fresnel zone equal to 2.5 m), and 1.2 m^3 for the 200 MHz antennas (Fresnel zone of 0.9 m). The observed wave velocity, and hence hydraulic conductivity, is an average of the porous medium within the Fresnel volume.

Figure 8 illustrates the relationship between measured hydraulic conductivity and the test support volume. The hydraulic conductivity increases with the support volume up

to an upper bound, after which the hydraulic conductivity remains approximately constant and the medium may be considered quasi-homogeneous. This upper bound occurs at a volume of approximately 10^4 m^3, but is highly dependent on the type of porous media (Schulze-Makuch et al. 1999). We have assumed the upper bound for this outwash is represented by the hydraulic conductivity obtained from the pumping test that has a support volume of 1.36×10^4 m^3. Included in Figure 8 is a value of hydraulic conductivity we determine, in a later section of this paper, from the observed thermal plumes at this site. The data below the upper bound vary as some power of the support volume (Neuman, 1994) and may be described by the empirical relationship

$$K = cV^m, \qquad [9]$$

where c is a coefficient characteristic of the porous medium, V is the support volume, and m is a scaling exponent (Schulze-Makuch et al., 1999). From a regression of the eight data points c is $10^{-2.84}$ and m is 0.22. The correlation coefficient r of the relationship is 0.92. From Eq. [9] the value of hydraulic conductivity may be estimated at any scale of interest. The value we determine for m of 0.22 is less than 0.5 reported for glacial outwash sediments in Wisconsin (Schulz-Makush et al., 1999), but it is within the range reported by Schulz-Makush and Cherkauer (1998). This suggests one should exercise caution when applying this relationship at sites where the coefficients have not been determined with site-specific data.

While hydraulic conductivity increases with measurement scale, the variance of ln(K) decreases as larger and larger heterogeneities are averaged by the test. Our data from the falling-head test is the exception having the smallest support volume and variance. Two factors may have contributed to this. The diameter of the piezometer tubes for these tests was 0.0095 m and the small diameter may have restricted the flow within the piezometer tubes, resulting in a lower estimate of hydraulic conductivity (Butler, 1997). The narrow distribution of the falling-head-determined conductivities probably results from the zone of disturbed aquifer surrounding the piezometer. Drilling and well installation mixes the aquifer material around the piezometer. As a result, the falling-head test yields hydraulic conductivity values that are less variable and biased by this disturbed zone toward the mean hydraulic conductivity of the porous medium. These factors must be considered when using the falling-head test data.

The observed increase in hydraulic conductivity with support volume illustrates the need for considering the scale of the field problem under investigation and carefully selecting methods for measuring hydraulic conductivity that will ensure they meet the needs of the investigation. While methods for up scaling have been proposed, they should be used judiciously and supported by the collection and analysis of site-specific data.

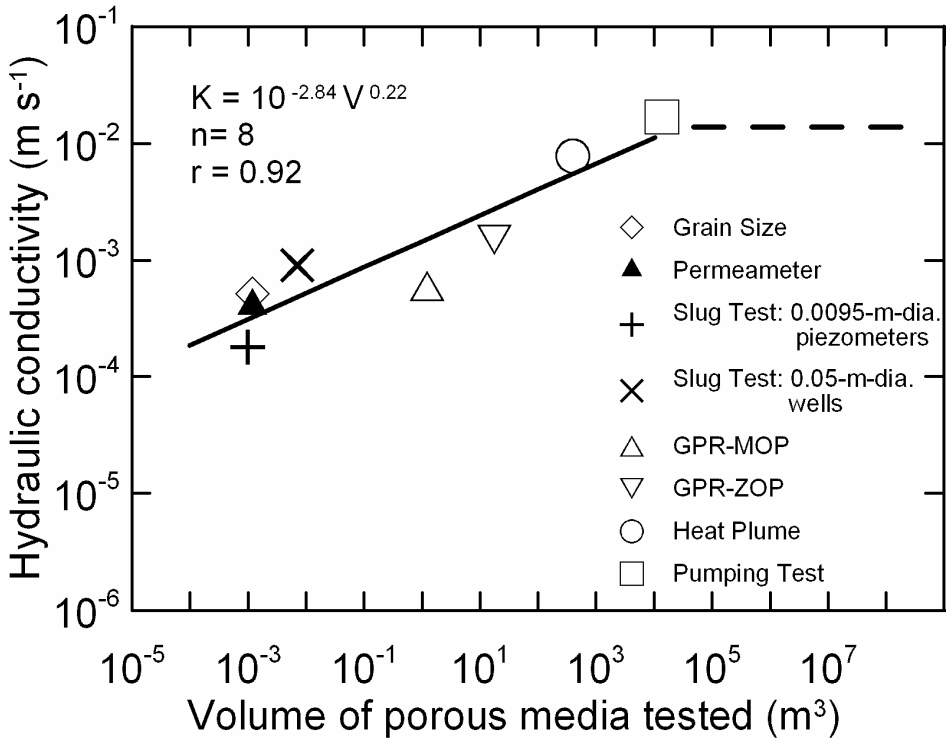

Figure 8 Relationship of hydraulic conductivity to scale of measurement in glacial outwash sand and gravel. The upper bound, shown by the dashed line, is assumed to be the hydraulic conductivity obtained from the constant-rate pumping test which has a support volume > 10^4 m^3 (Schulz-Makuch et al., 1999).

Aquifer thermal properties

We calculated the mean heat capacity of the aquifer solids C_s from the known mineral composition, and values for the specific heat and density of the mineral phases (Table 4) using Eq. [3]. The estimated heat capacities have a narrow range from 2.205×10^6 J m^{-3} K^{-1} for the average value for sand to 2.235×10^6 J m^{-3} K^{-1} for both gravel and till (Table 5), suggesting that a value of 2.22×10^6 J m^{-3} K^{-1} is representative of the heat capacity of the aquifer solids. Assuming values of 4174 J kg^{-1} K^{-1} and 1000 kg m^{-3} for the specific heat and density of water, respectively (de Vries, 1963), and a porosity of 0.29, we estimated the heat capacity and 95% confidence interval of the saturated aquifer to be $(2.79 \pm 0.01)\times10^6$ J m^{-3} K^{-1}.

Table 4. Values of specific heat and density for minerals found in the outwash and till.

Mineral	Specific heat c_s				Density ρ	
	Čermák and Rybach (1982)	Mercer et al. (1982)	Robie et al. (1978)	Helgeson et al. (1978)	Horai (1971)	Clark (1966)
	J kg^{-1} K^{-1}				kg m^{-3}	
Calcite	793	786	834	818	2721	2712
Dolomite			854	853	2857	2866
Anorthite	700		760	757	2769	2762
Hornblende		817			3254	
Quartz	698	787	690	740	2647	2533
Clay minerals	870				2900	2834

Thermal conductivity of the aquifer solids λ_s, determined from the divided bar apparatus, ranged between 3.38 and 4.81 W m^{-1} K^{-1}. The thermal conductivities are normally distributed (Shapiro-Wilk test, $W^*_{.05,41} = 0.941 < W = 0.982$, with p value = 0.7) and the mean value and 95% confidence interval are 4.09±0.09 W m^{-1} K^{-1}. The standard deviation of the measured values is 0.29 W m^{-1} K^{-1}. We found λ_s was dependent on the grain size and mineral composition of the porous medium and could be assigned to three groups; till, gravel, and fine to coarse sand (Markle et al., 2006). The mean values of λ_s for these groups are summarized in Table 5.

Table 5. Average thermal properties of the porous medium solids

Source	Thermal conductivity of porous medium solids, λ_s Mean ± C.I.†			Heat capacity of porous medium solids, C_s Mean ± C.I.		
	Sand	Gravel	Till	Sand	Gravel	Till
	W m^{-1} K^{-1}			kJ m^{-3} K^{-1}		
Mineral composition	3.99 ± 0.16 (17) ‡	3.83 ± 0.13 (6)	4.05 ± 0.14 (3)	2205 ± 25 (17)	2235 ± 14 (6)	2235 ± 36 (3)
Divided-bar apparatus	4.22 ± 0.10 (24)	3.94 ± 0.12 (11)	3.72 ± 0.59 (4)			

† 95% confidence interval.
‡ The number of samples n used to determine the average value.

The apparent thermal conductivity λ, of a porous medium can be estimated by a variety of empirical equations and mixing formulas (e.g., Woodside and Messmer, 1961; Hashin and Shtrikman, 1962; de Vries, 1963; Johansen, 1975; Campbell et al., 1994). Using Akaike's information criterion (Akaike, 1973), we found the Campbell et al. (1994) model to be the best-approximating model for the porous medium at this site (Markle et al., 2006). Using the Campbell model we obtained estimates of apparent thermal conductivity in the saturated aquifer ranging from 2.14 to 2.69 W m^{-1} K^{-1} with a mean of 2.42 W m^{-1} K^{-1}. We estimated λ in the till to be 1.90 W m^{-1} K^{-1}. In the unsaturated zone, λ ranged from 2.6 W m^{-1} K^{-1} in the capillary fringe (estimated from grain size distributions to be 0.01–0.05 m above the water table) to 1.4 W m^{-1} K^{-1} at the ground surface. In the unsaturated zone, λ varies directly with the moisture content.

We also estimated λ using the background temperature profiles collected at the up gradient multilevel well, M0 (Fig. 9). As a periodic temperature variation propagates

through the subsurface, the amplitude of the temperature variation decreases with depth while the time lag t_d, between the peak temperature at depth z and the ground surface, increases with depth. Assuming heat transport from the surface vertically through the aquifer is mainly by conduction, the time lag is

$$t_d = \left(\frac{z}{2}\right)\left(\frac{PC_0}{\pi\lambda}\right)^{1/2}, \qquad [10]$$

where P is the period of the temperature variation (Ingersoll et al., 1954). The velocity at which the temperature variation propagates through the aquifer is

$$\frac{z}{t_d} = 2\left(\frac{\pi\lambda}{PC_0}\right)^{1/2}. \qquad [11]$$

In a homogeneous medium, plotting z versus t_d yields a straight line with a slope equal to the right-hand side of Eq. [11]. A plot of z versus t_d obtained for the nine thermistors within the saturated zone yields a fitted line with a slope of 0.0506 m d^{-1} and a coefficient of determination r^2 of 0.976. Given a period of 365 d and a heat capacity of 2.79×10^6 J m^{-3} K^{-1}, the apparent thermal conductivity of the saturated porous medium is estimated to be 2.40 W m^{-1} K^{-1}, which is in excellent agreement with the average value of 2.42 W m^{-1} K^{-1} we estimated using the Campbell et al. (1994) model. Use of this method assumes that vertical heat transport is by conduction only with no convective heat transport. During large infiltration events, such as spring snowmelt and increased precipitation in the late fall, this assumption may not be valid. Under these conditions, the apparent thermal conductivity will be over-estimated. Lag times may be determined by comparing the times at which maximum or minimum temperatures occur at the depths of interest. If these peaks are influenced by significant recharge events, the lag times may be biased due to convective heat flux. To reduce the influence of individual recharge events on our estimates of time lag, we made use of the entire temperature record by cross-correlating the surface temperature signal with those measured at depth. As well, we investigated the influence that convective heat transport, due to vertical flow from recharge, may have on estimates of apparent thermal conductivity using the solution to the conduction–convection heat transport equation proposed by Stallman (1965). We completed simulations using a thermal conductivity and heat capacity of 2.4 W m^{-1} K^{-1} and 2.79×10^6 J m^{-3} K^{-1}, respectively, for the saturated aquifer with vertical fluxes ranging from 0 m s^{-1} (pure conduction) to 1.27×10^{-7} m s^{-1} (4000 mm yr^{-1}). Following the procedure outlined above and plotting z versus t_d, we obtained estimates of apparent thermal conductivity that were within 1% of the true conductivity provided the flux was $<6.34\times10^{-8}$ m s^{-1} (2000 mm yr^{-1}). For flux rates of 1.27×10^{-7} m s^{-1}, the estimated apparent conductivity was 5% larger than true conductivity. The recharge rate at this site is between 300 and 400 mm yr^{-1}. This suggests that the apparent thermal conductivity we estimated using this method, will not been influenced significantly by the convective transport of heat vertically through the subsurface.

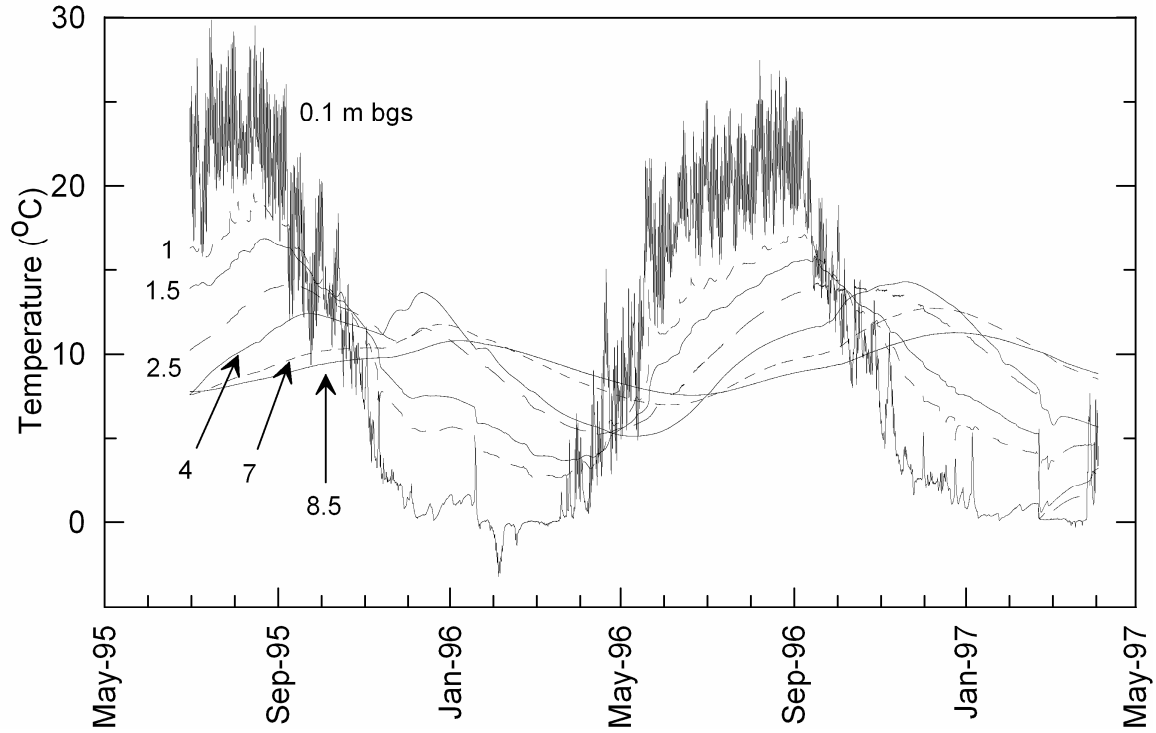

Figure 9 Temperature profile for the up-gradient multilevel well M0. The depths of the thermistors are reported as metres bgs (below ground surface). For clarity, the temperatures for only seven of the 12 thermistors are shown.

Water level monitoring

The observed water levels in the pond (Fig. 10) and two down-gradient monitoring wells (M8 and M13) suggest the hydraulic head in the aquifer is controlled mainly by seasonal and short term variations in precipitation. During the 22-month monitoring period, the water table fluctuated by 0.7 m resulting in a 10% variation in the saturated thickness of the aquifer and yielding an average saturated thickness of ~5 m. The horizontal gradient between the pond and M13 ranged from 9×10^{-4} to 1.5×10^{-3} m m^{-1}, and the mean annual hydraulic gradient is estimated to be $(1.2 \pm 0.1)\times10^{-3}$ m m^{-1}. While the calculated mean annual vertical gradients were generally $<5\times10^{-4}$ m m^{-1}, in most cases the observed head differences were smaller than the uncertainty in measured water levels (±0.003 m). Therefore, we do not consider the calculated vertical gradients to be significantly different from zero. During large recharge events, such as spring snowmelt, we observed vertical gradients as large as 0.3 m m^{-1}, but these gradients quickly returned to near zero after recharge ceased. Thus, the hydraulic head distributions we observed suggest that flow through the outwash aquifer is predominantly horizontal.

With an average porosity of 0.29 and using the hydraulic conductivity from the constant discharge test of 1.7×10^{-2} m s^{-1}, the estimated average linear ground water velocity at 10°C is 7×10^{-5} m s^{-1} (6.1 m d^{-1}). For the streambed piezometers, the average vertical hydraulic gradient was –0.1 m m^{-1} at each location (negative values indicating discharging conditions), and discharging conditions were predominant throughout the year.

Air – ground surface temperature and heat flux

The air temperature, near-surface soil temperature, and soil heat flux measured at M14, are shown in Figure 11. The mean annual air temperature, measured 2 m ags, was 7.6ºC with minimum and maximum daily average values of –19.5ºC and 27.6ºC, respectively. The mean annual soil temperature at 0.02 m bgs was 10.9ºC, with minimum and maximum daily average temperatures of –7.9ºC and 30.2ºC, respectively. The average annual near-surface soil temperature is 3.3ºC higher than the air. This has been observed in a number of studies (e.g. Beltrami, 2001; Schmidt et al., 2001; Zhang et al., 2001) and several empirical relationships predict a 1–3ºC difference between air and soil temperature (e.g. McDole and Fosberg, 1974; Kluender et al., 1993; Isard and Schaetzl, 1995). This difference is due to several factors including the heating of the soil by the solar radiation, the greater heat capacity of the soil compared to the air, and the insolating effect of the snow cover during the winter which decouples the soil temperature from the air temperature. Furthermore, the heat exchange across the ground surface is seasonally variable, and depends on the stage of vegetation growth and the amount of snow cover. The soil heat flux reaches maximum values in July and August ranging from up to 180 W m^{-2} during the day down to –70 W m^{-2} at night (Fig. 11c). In the winter (December to March), the heat flux drops to near zero due to the insulating effect of the snow cover, the suppression of conductive heat transport through the release of latent energy during soil freezing, and the zero-curtain effect caused by water infiltration during spring snowmelt (e.g. Goodrich, 1982; Outcalt et al., 1990; Kane et al., 2001; Smerdon et al., 2003). During this period, there is little heat exchange between the air and near surface soils. These data show that heat flux across the ground surface is seasonally variable and that the air temperature may not be representative of the near-surface soil temperature. Where possible, direct measurements of the near-surface soil temperatures and heat flux should be collected.

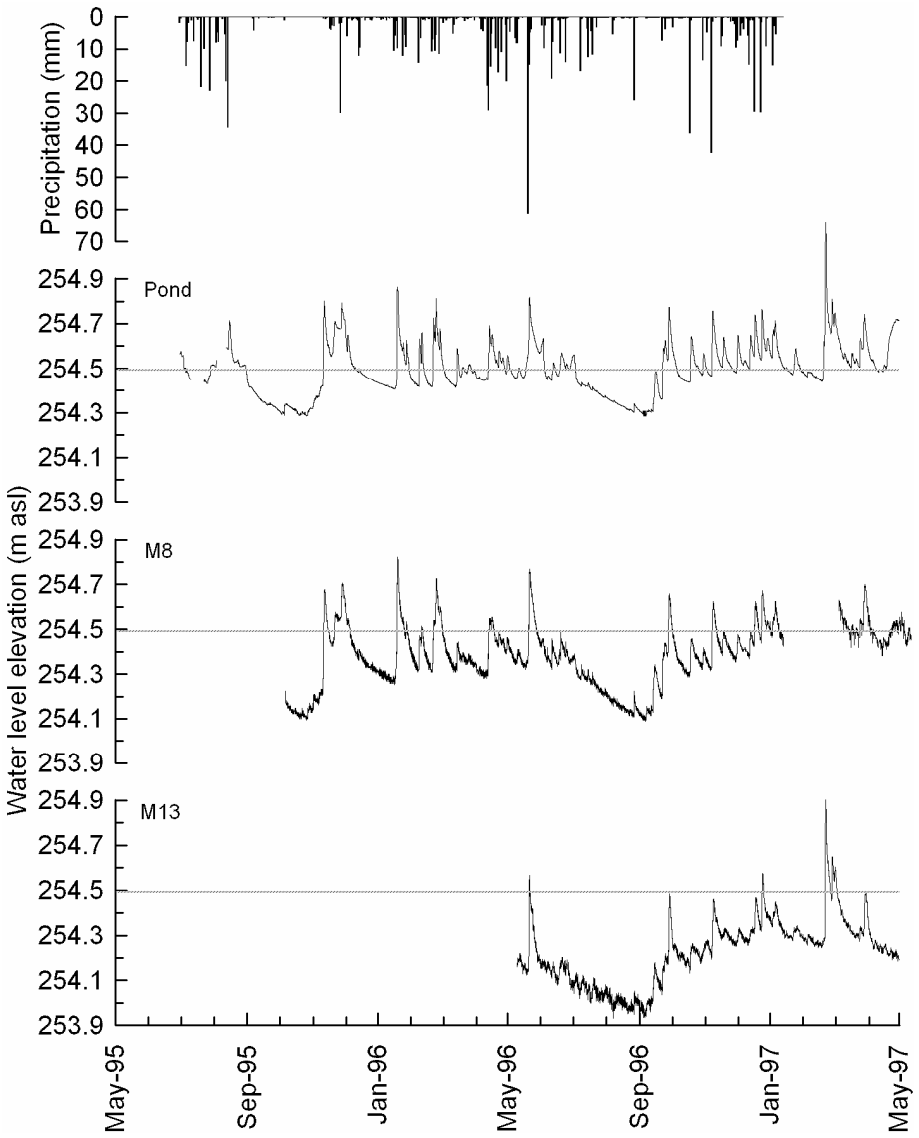

Figure 10 Water levels in the pond and two down-gradient monitoring wells (M8 and M13). Precipitation is shown at the top.

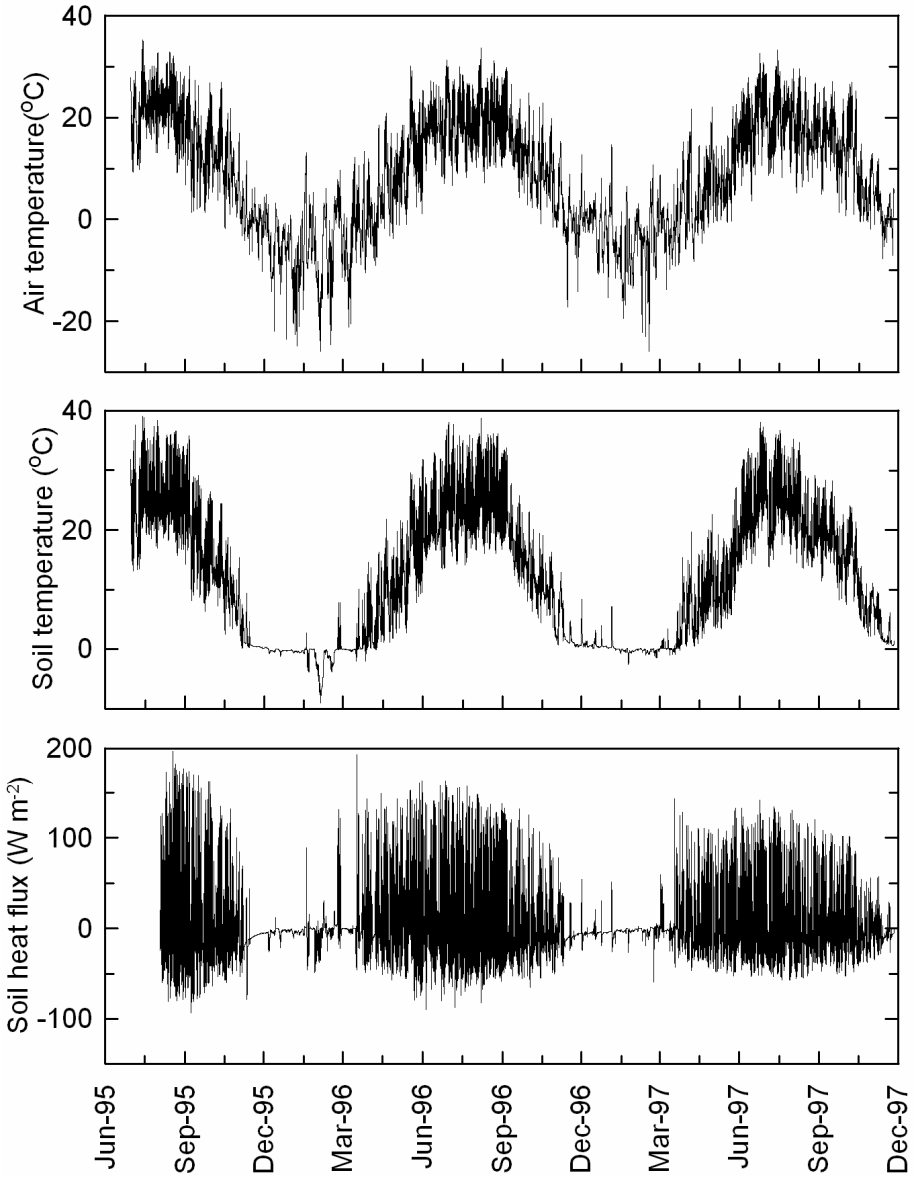

Figure 11 Shown are: (top) air temperature at 2 m ags (above ground surface), (middle) near-surface soil temperature 0.02 m bgs (below ground surface), and (bottom) soil heat flux 0.05 m bgs at M14.

Pond water temperatures

The pond temperatures show the magnitude of the thermal perturbation caused by the presence of the pit (Fig. 12). The water temperature near the surface of the pond ranges from near 0°C in February to over 30°C in August. The pond is stratified for about five months of the year between the beginning of May, when the surface of the pond begins to warm, and mid- to late September, when the pond begins to cool. For the remainder of the year the temperature is uniform throughout the depth. At the pond surface, the mean annual temperature is 11.7ºC and the amplitude is 30ºC (0.5–30.5ºC). Near the bottom of the pond (5.65 m below the pond surface), the average temperature is 10.4ºC and the amplitude is attenuated by ~31% relative to the surface temperature and is 20.6ºC (2.1–22.7ºC). The pond temperature is uniform during the winter (December to March) and has an average temperature of 4ºC. In contrast, the annual temperature amplitude of the ground water is much smaller at M0, located approximately 27 m up gradient of the pond (Fig. 9). At a depth of 0.1 m bgs, the mean annual soil temperature at M0 is 11ºC and the amplitude is 20.9ºC (2.1–23.0ºC). At a depth of 6 m bgs (equivalent to the bottom thermistor in the pond), the mean temperature at M0 is 9.3ºC and the amplitude is 4.8ºC (7.0–11.8ºC) and has been attenuated by ~77% relative to the surface temperature. The lower attenuation of the surface temperature wave in the pond in comparison to the aquifer markedly alters the natural thermal regime. This temperature perturbation in the pond moves into the aquifer down gradient of the pond as shown in the following sequence of figures.

Thermal plume monitoring

Figure 13 shows the temperature distribution in the aquifer during a one-year period. These results, collected in the first 22-month monitoring period, show two distinct thermal pulses moving from the pond through the aquifer – a cool winter pulse followed by a warm summer pulse. The plumes persist above background ground water temperature for up to 250 m down gradient of the pond, and for a period of 11-months after entering the aquifer. Between December and March the low rate of heat exchange across the ground surface is evident by the temperature of the near-surface soil which is relatively stable compared to the remainder of the year. During this period the plume temperature is not moderated by heat exchange across the ground surface. Other significant features are the annual surface temperature wave moving down into the aquifer in the summer and fall, and the overall cooling of the aquifer in April. This cooling is the result of the combined effect of the latent heat of melting of the snow and ice, which absorbs heat from the aquifer, and the convective flux of cold water infiltrating into the aquifer after the spring snowmelt.

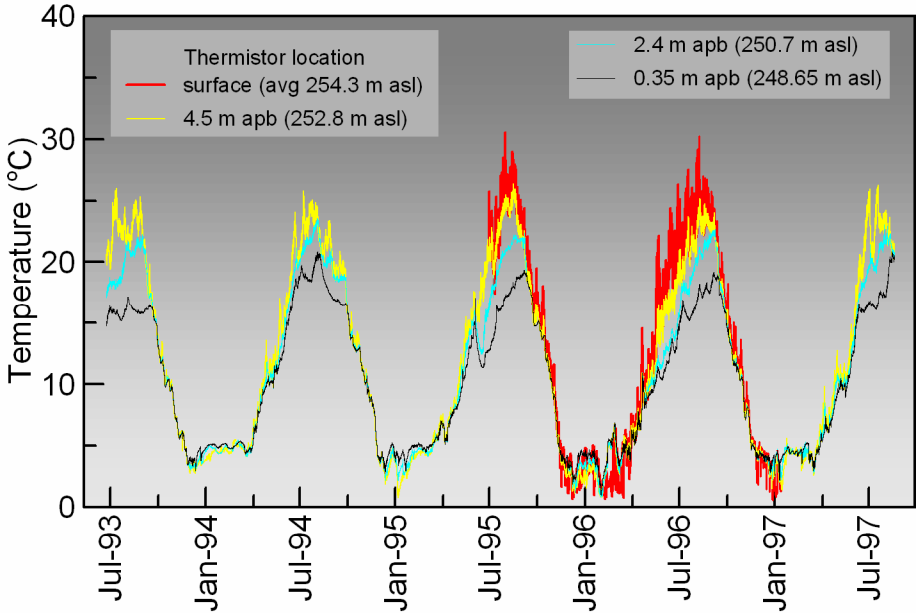

Figure 12 Pond temperature profile at the surface and 4.5, 2.4, and 0.35 m apb (above the pond bottom).

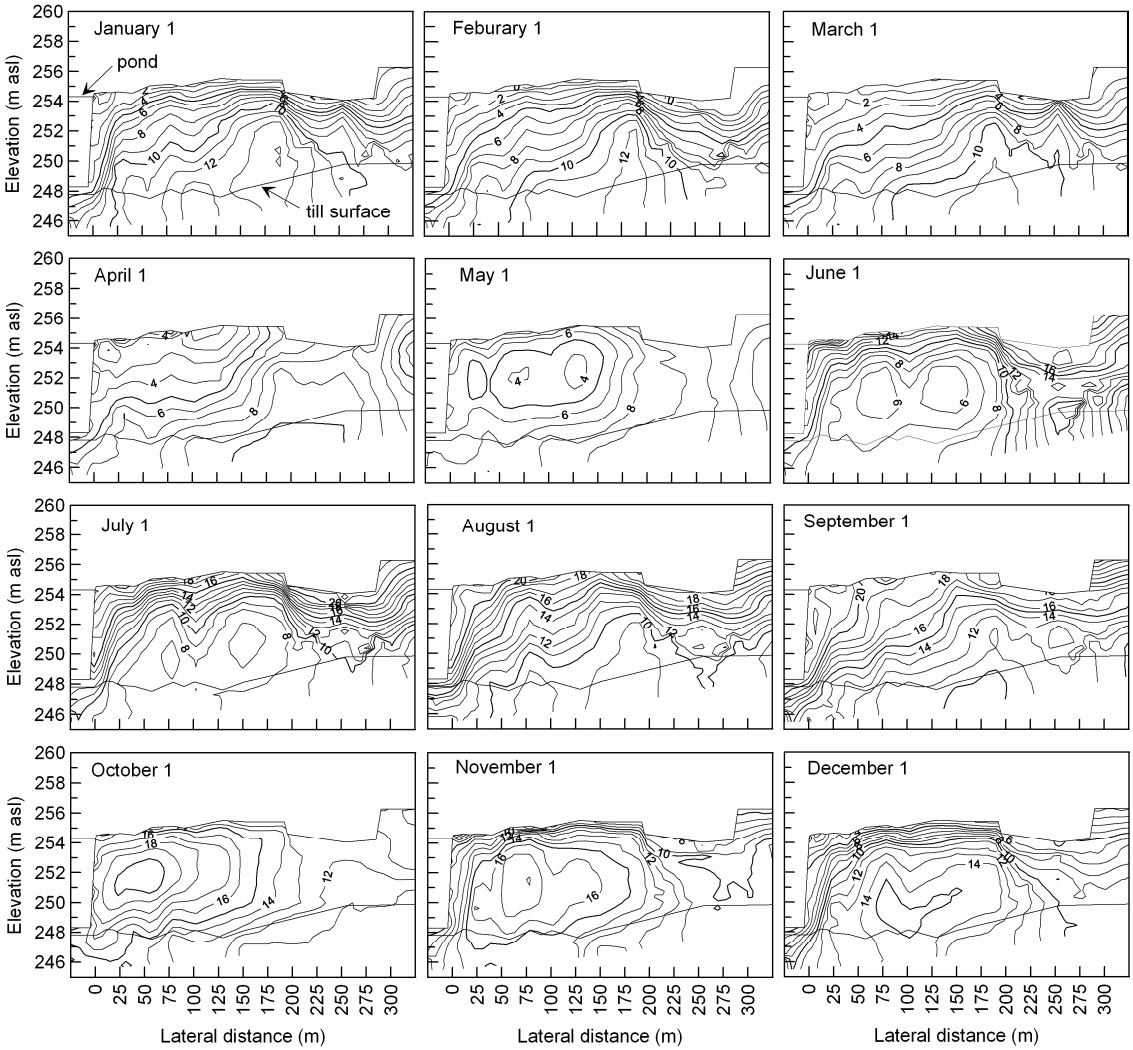

Figure 13 Thermal plume migration along section A–A' for period January to December 1996.

Much like chemical tracer tests, we can use the observed thermal plumes to estimate the plume transport rate and gain insight into the influence of thermal retardation on this rate. To estimate the plume transport rate, we cross-correlated the periodic temperature signals measured in the pond with the temperature signals measured at similar elevations in the aquifer. However, as the annual temperature variation in the pond moves horizontally through the aquifer mainly by convection with the ground water flow, it combines with the annual surface temperature variation, moving vertically through the aquifer mainly by conduction. As these two temperature signals combine, the thermal plume from the pond is gradually attenuated (e.g., the warm thermal plume entering the aquifer from the pond in the summer is cooled by the cold temperature wave moving from the surface in the fall and winter), and identifying the pond signal within the observed temperature signal in the aquifer becomes increasingly difficult as the distance down gradient from the pond increases. As well, any convective heat flow vertically into the aquifer will tend to enhance the plume attenuation. Cross correlation of the temperature signals measured at a depth of approximately 4.5 m bgs (250 m asl), provided good estimates of lag times for wells within the first 80 m of the aquifer (Table 6).

Table 6. Lag times determined from cross-correlation of the periodic annual temperature variation in the pond with the periodic temperature variation in the aquifer down gradient of the pond.

Well	Distance from pit face	Lag time†	Maximum lag value	Standard error of cross–correlation	Plume velocity
	m	d			m d^{-1}
M2	11.2	7.8	0.972	0.0456	0.7
M3	18.2	32.9	0.926	0.1321	1.8
M4	24.9	34.8	0.914	0.1430	1.4
M5	40.2	44.9	0.902	0.1784	1.1
M6	79.2	66	0.871	0.2539	0.8

† Lag times are for temperatures measured near the bottom third of the aquifer at a depth of approximately 4.5 m bgs (250 m asl).

For our analysis, we considered the results of the cross-correlation to be good provided the maximum lag value was >0.85 (where a lag value of 1 is a perfect fit) and the standard error was <0.3. For the wells beyond 80 m, we found cross-correlation became less reliable as the lag value decreased and the standard error increased. Using data from the first 80 m, the lag times yield an average observed plume velocity of approximately 1.2 m d^{-1}. This observed plume velocity is less than the ground water velocity, due in part to attenuation of the thermal plume by vertical heat transport, but more importantly due to thermal retardation resulting from the contrast between the heat capacity of the porous medium solids and the pore water. The thermal retardation factor R is given by

$$R = \frac{C_0}{S\phi c_w \rho_w} \qquad [12]$$

where S is the saturation, and the plume migration velocity is

$$v_p = \frac{v}{R}, \qquad [13]$$

where ν is the average linear ground water velocity. With an average porosity of 0.29, an estimated heat capacity C_0 for the saturated aquifer of 2.79×10^6 J m^{-3} K^{-1}, and assuming values of 4174 J kg^{-1} K^{-1} and 1000 kg m^{-3} for the specific heat and density of water, respectively, the estimated retardation factor is 2.3. This agrees well with values of *R* obtained in similar aquifer materials: 2.0 for fine sands and 2.3 for sands and gravel (Andrews and Anderson, 1979); 1.9 for the Borden sand (Molson et al., 1992), and 2.0 for sands and gravels (Parr et al., 1983). These data suggest that the range of values for *R* is narrow for saturated sand and gravel aquifers and, as a first approximation, it may be reasonable to assume *R* is equal to 2. For *R* equal to 2.3, we estimate the average ground water velocity to be 2.8 m d^{-1}, about half the value of 6.1 m d^{-1} estimated from the hydraulic conductivity measured by the constant discharge test. This difference may be related to the difference in support volumes (Table 3) and the differences in the dimensionality of the tests. As shown by stochastic theory (Gelhar, 1993) and theoretically (Neuman, 1994) the effective hydraulic conductivity depends on the dimensionality of the test. Rovey and Niemann (2001) suggest that in heterogeneous aquifers tracer tests measure a two-dimensional hydraulic conductivity that is the geometric mean of the hydraulic conductivity field, while pumping tests measure a three-dimensional conductivity that is larger and lies between the geometric and arithmetic mean. Thus use of the hydraulic conductivity measured by the pumping test may overestimate the thermal plume velocity.

Ground water – surface water interaction

The ground water temperatures that we measured suggest that the thermal plumes at this site reach background temperatures after migrating ~250 m through the gravel and sand aquifer. The nearest stream is ~400 m down gradient of the pit and Tricks Creek is ~750 m. Thus, the thermal effects from this pit are not impacting the surface water temperatures in either the tributary or Tricks Creek; however, as extraction proceeds south toward the tributary and Tricks Creek, impacts may occur. In addition there are several active pits within the watershed (Fig. 3) that could alter the stream temperature if adequate separation distances are not maintained. Thermal changes that Tricks Creek and associated tributaries can tolerate must be quantified before appropriate resource management decisions can be made. As a first step toward this objective, we measured the stream temperature and the ground water temperature (1 m below the streambed) at four locations within the watershed; MP1, MP2, MP4, and MP5 (Fig. 14a–14d). For MP1, MP2, and MP4, data for the period July 1995 to May 1997 are shown, and for MP5 data for the period December 2004 to June 2006 are shown. MP1, MP2, and MP5 are located in the upper reaches of the watershed where we typically expect temperature conditions to be suitable for spawning and incubation. The streambed at both MP1 and MP5 is, however, fine grained making these sites unsuitable for spawning. The streambed at MP2 and MP4 is predominantly gravel and thus suitable for spawning. We have presented the data for MP1 and MP5 to emphasize the variation in the ground water – surface water interactions across the watershed.

For both benthic invertebrates and fish, the critical habitat requirements are concentrated largely in the early stages of development. For fish this includes the spawning and early rearing periods (Baxter and McPhail, 1999), and for macroinvertebrates this includes the egg and pupal development stages (Vannote and Sweeney, 1980). The thermal requirements for brook trout are given in Figure 14. Temperature data for macroinvertebrates are not as detailed as for brook trout. Of the macroinvertebrates found in Tricks Creek (Ephemeroptera, Plecoptera, Trichoptera, and Diptera), Plecoptera and Trichoptera are the most temperature sensitive. These two freshwater invertebrates tend to be restricted to cool-water habitats with a temperature range of 0–20ºC (Quinn et al., 1994; Hogg and Williams, 1996). The upper lethal temperature for many cool-water insects is <24ºC (Nebeker and Lemke, 1968; Gaufin and Hern, 1971, deKozlowski and Bunting, 1981; Quinn et al., 1994). While these data provide upper limits on the range, several studies have shown that small temperature changes alter the structure of the macroinvertebrate community. For example, a large scale field experiment conducted in a first order cool-water stream in southern Ontario, showed that mean annual temperature changes as small as 2.1–2.4ºC result in measurable changes that adversely affected the invertebrate community (Hogg and Williams, 1996). Other studies have reported measurable differences in growth rates for Ephemeroptera and Tricoptera for temperature changes of only 2ºC (Vannote and Sweeney, 1980), while a temperature difference of 4ºC (above the mean of 8.4ºC) virtually eliminated a mayfly in the family leptophlebiidae (Rempel and Carter, 1986). These data suggest that temperatures below 20ºC are desirable and that small changes (2–4ºC) may adversely affect macroinvertebrates found in cool, headwater streams.

Figure 14a–14c show that the ground water moderates the stream temperature by discharging water that is cooler in the summer and warmer in the winter than the stream temperature at sites MP1, MP2, and MP4. The annual temperature amplitude of the discharging ground water at MP5 is larger than at the three other sites and is nearly the same as the amplitude for the stream. We believe this is due to different discharge conditions at MP5. Here the floodplain is 90-m wide and the stream lies along the southern edge. At this location, the stream is not incised as much as it is at the other sites. In the floodplain, a 0.5–1 m thick silt layer, blanketed by approximately 0.5 m of peat and muck, overlies the sand and gravel aquifer. The silt layer restricts the ground water discharge in to the stream. As a result, ground water discharge is diffuse within the riparian zone where it mixes with infiltrating precipitation and enters the stream as near-surface flow through the soil and peat in the floodplain. Thus in the summer, the ground water warms as it flows laterally through the peat and mixes with infiltration, prior to entering the stream. The warm discharging ground water and the fine streambed substrate at MP5 result in conditions that are poor for spawning.

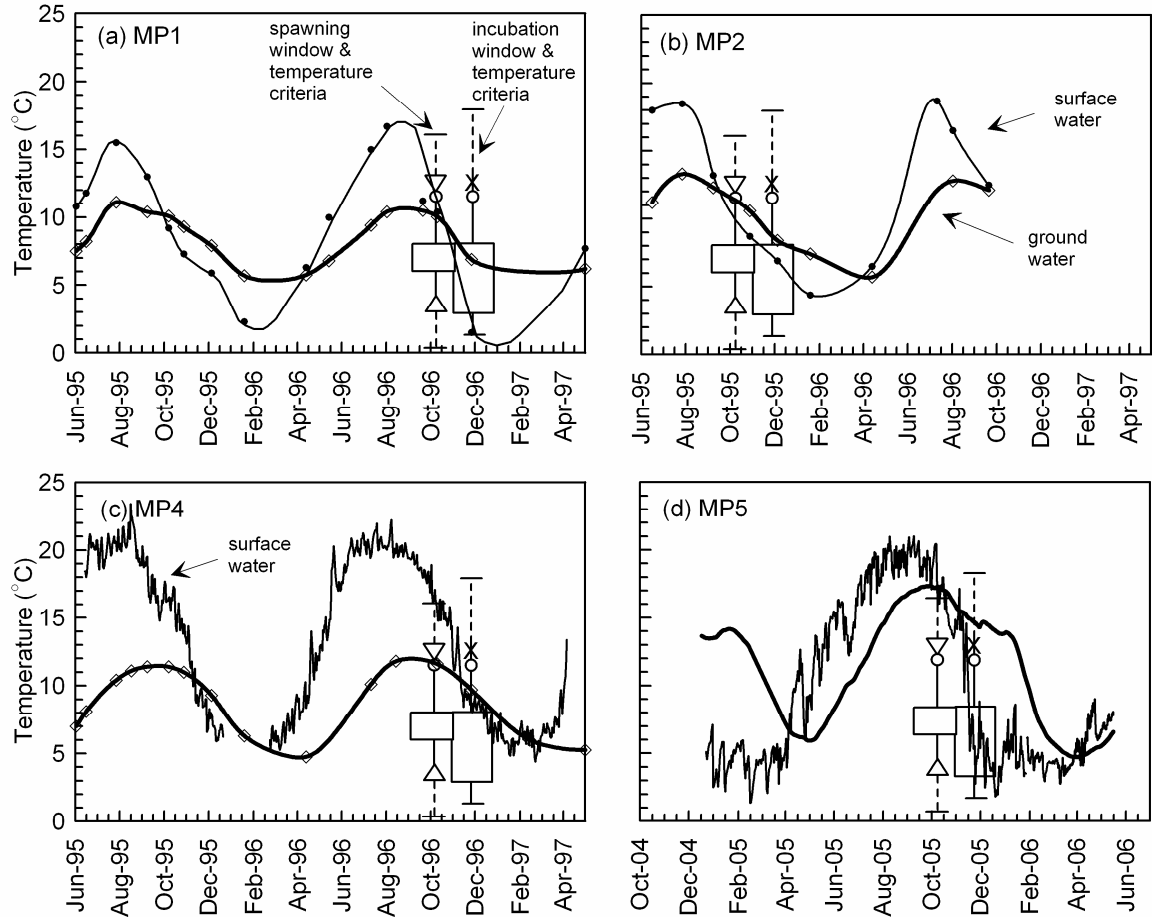

Figure 14 Surface water temperature and ground water temperature (1 m below the base of the streambed) at (a) MP1, (b) MP2, (c) MP4, and (d) MP5. Also shown are the spawning and incubation time periods and temperature criteria for brook trout. The top and bottom of the boxes define the optimum temperature range for spawning and incubation (Hokanson et al., 1973; Witzel and MacCrimmon, 1983), and the width defines the time period during which spawning and incubation commonly occur. The open triangles define the upper and lower temperatures at which brook trout commonly spawn in Ontario (Witzel and MacCrimmon, 1983). The open circle shows the ET50 (Hokanson et al., 1973; Scott and Crossman, 1973), which is the upper mean effective temperature giving the median sublethal response, and the × shows the LT50 (Hokanson et al., 1973) which is the temperature at which 50% normal hatch occurs. Finally, the horizontal bars indicate the temperatures beyond which spawning and incubation are unsuccessful (Hokanson et al., 1973; Curry et al., 2002.

Brook trout begin spawning in mid-September and continue until mid- to late November. At all these sites except MP5, the temperature in the hyporheic zone ranges between 8.5ºC and 13ºC during October and November. By mid-November, the ground water is approximately 2ºC warmer than the surface water. The measured stream and ground water temperatures show that the temperatures at MP1 are within the optimum ranges for spawning and incubation, and at MP2 they are within the range brook trout commonly spawn. At MP4 the stream temperature is near the maximum range. At MP5, both ground water and surface water exceed the maximum temperature. In the winter (December to March), the average surface water temperature is 4ºC but drops to about 1ºC on occasion. While temperatures <1ºC can be tolerated by incubating brook trout (Curry et al., 2002), in areas of low ground water discharge egg mortality increases dramatically (Curry et al., 1995; Power et al., 1999). During the winter, the mean ground water temperature remains between 6ºC and 8ºC at MP1, MP2, and MP4. This warm ground water maintains the water temperature in the hyporheic zone within or near optimum incubation temperatures, prevents the formation of anchor ice, and provides thermal conditions suitable for alevin growth prior to emergence from the substrate in late March to early April. Under these temperature conditions the incubation period is approximately 60 d (Garside, 1966). In the summer (June to September) the ground water is between 5ºC and 10ºC cooler than the surface water. This provides thermal moderation of the high surface water temperatures, particularly during July and August.

These data highlight the importance of the temperature of the discharging ground water on the spawning and incubation conditions. While not all the locations we monitored are used for spawning, ground water temperature increases of only 2–3ºC would shift water temperatures outside of the acceptable ranges. In particular, at MP5 even a small increase in ground water temperature in the fall would push temperatures well above the maximum temperatures for spawning. At MP4, an increase of 1–2ºC in ground water temperature would result in temperatures that exceed the LT50 for incubation. These small temperature changes could alter the structure of the biotic communities by reducing the benthic invertebrate diversity, adult size and fecundity, and adversely affecting the productivity of the stream by decreasing the survivability of the fish eggs and alevins. Thus, even small temperature changes may cause unacceptable impacts to the biotic community within this creek. This suggests that the setback between aggregate pits and sections of the creek used for spawning should exceed 250 m, recognizing that larger setbacks will be required where ground water velocities are higher.

Summary and Conclusions

We observed thermal plumes migrating through a glacial-outwash sand and gravel aquifer in which the ground water velocity is approximately 2.8 m d^{-1}. The average apparent thermal conductivity of the outwash sand and gravel is 2.42 W m^{-1} K^{-1} and the thermal retardation factor was estimated to be 2.3. In this aquifer, the thermal plume velocity (~1.2 m d^{-1}) is less than half the ground water velocity due to thermal retardation. Under these conditions the cool and warm thermal plumes persist for up to 11

months after entering the aquifer and migrate up to 250 m down gradient. At this site, the ground water discharges to streams that are well beyond this distance, and thus are not affected by these thermal plumes. If, however, within this zone a stream was present and aquatic animals such as brook trout and cool-water macroinvertebrates were relying on the cool ground-water discharge, then thermal alterations may adversely affect these animals.

Our results indicate that laboratory-measured hydraulic conductivities are up to two-orders of magnitude smaller than field-measured hydraulic conductivities for this heterogeneous glacial outwash aquifer. The laboratory-measured hydraulic conductivities should be considered lower bounds on the aquifer hydraulic conductivity. Our data show that large-scale field-measured hydraulic conductivities will provide better estimates of hydraulic conductivity for predicting thermal plume velocities; however, velocities estimated with hydraulic conductivity from pumping tests may overestimate plume velocities and should be considered an upper bound on the hydraulic conductivity. While methods of scaling between laboratory-measured and field-measured hydraulic conductivities may be useful, one should verify the validity of the relationship for a particular site with multi-scale, site-specific data.

In this watershed, the temperature of the discharging ground water ranges between 5°C and 17°C and moderates the stream temperatures. Comparison of the measured temperatures within the hyporheic zone and the stream shows that temperature changes of 2–3°C could shift temperatures beyond the maximum temperatures for brook trout spawning and adversely alter the structure of the macroinvertebrate community. These data emphasize that even small temperature changes may adversely impact the stream productivity especially if the stream temperatures are already near the upper or lower tolerable temperatures. As shown here, temperature conditions vary across the watershed. Establishing the thermal regime within the stream, the interaction of the ground water and surface water, the spatial distribution of thermally sensitive aquatic animals, and the linkages to the stream environment is necessary to assess potential impacts on stream productivity from thermal disturbances to the discharging ground water. Given the potential for small changes in ground water temperature to negatively impact the benthic and fish community in this creek, quantification of the transport distance of the thermal disturbance from the aggregates pits is very important so that informed conservation and resource management decisions can be made.

This study demonstrated that aggregate extraction can impact stream temperatures if sufficient separation distances are not provided, and that these temperature changes may adversely affect the macroinvertebrate community and incumbent brook trout populations. The cumulative effects of several operations within the watershed are still unknown. Quantifying these effects will require a highly integrated study so that we may understand the ground water – surface water interaction within the watershed and the links to the ecology in the context of the stream environment.

Acknowledgments

We are grateful to Tom Sinclair, Township of Goderich, for providing access to the site, Kent Novakowski for providing drilling equipment in the initial phases of the investigation and assistance with pond temperature measurements, John McNeil and Greg Powers for their assistance with the field work, and Ron Griffiths for providing his data on the macroinvertebrates. This work was funded by the Department of Fisheries and Oceans Canada, the Ontario Aggregate Resources Corporation, the Province of Ontario, the Natural Science and Engineering Research Council of Canada through grants awarded to R. A. Schincariol, student grants from the Geological Society of America, the American Association of Petroleum Geologists, and the Province of Ontario.

References

Acornley, R.M. 1999. Water temperatures within spawning beds in two chalk streams and implications for salmonid egg development. Hydrological Processes 13:439–446.

Akaike, H. 1973. Information theory as an extension of the maximum likelihood principle. p. 267–281. *In* B.N. Petrov and F. Csaki (eds.) Second symposium in Information Theory. Akadémiai Kiadó, Budapest.

Aldridge, D.F., D.W. Oldenburg. 1993. Two-dimensional tomographic inversion with finite-difference traveltimes. Journal of Seismic Exploration 2:257–274.

Anderson, M.P., J.S. Aiken, E.K. Webb, D.M. Mickelson. 1999. Sedimentology and hydrogeology of two braided stream deposits. Sedimentary Geology 129:187–199.

Andrews C.B., M.P. Anderson. 1979. Thermal alteration of groundwater caused by seepage from a cooling lake. Water Resources Research 15:595–602.

Barnett, P.J. 1992. Quaternary geology of Ontario. p. 1011–1088. *In* P.C. Thurston, H. R. Williams, R.H. Sutcliffe, and G.M. Stott (eds.) Geology of Ontario. Ontario Geological Survey, Special Volume 4, Part 2. Publications Ontario, Toronto, Ontario.

Baxter, J.S., J.D. McPhail. 1999. The influence of redd site selection, ground water upwelling, and over-winter incubation temperature on survival of bull trout (*Salvelinus confluentus*) from egg to alevin. Canadian Journal Zoology 77:1233–1239.

Beckie, R. 2001. A comparison of methods to determine measurement support volumes. Water Resources Research 37:925–936.

Beckie, R., C.F. Harvey. 2002. What does a slug test measure: An investigation of instrument response and the effects of heterogeneity. Water Resources Research 38 (12), 1290, doi:10.1029/2001WR001072.

Beltrami, H. 2001. On the relationship between ground temperature histories and meteorlogical records: A report on the Pomquet station. Global Planetary Change 29:327–349.

Boggs, J.M., S.C. Young, D.J. Benton, Y.C. Chung. 1990. Hydrogeologic characterization of the MADE site. Report EN-6915, Electric Power Resource Institute, Palo Alto, California.

Bradbury, K.R., M.A. Muldoon. 1990. Hydraulic conductivity determinations in unlithified glacial and fluvial materials. p. 138–151. *In* D.M. Nielsen and A.I. Johnson (eds.) Ground Water and Vadose Zone Monitoring, ASTM STP 1053. American Society for Testing and Materials, Philidelphia.

Brunke, M., T. Gonser. 1997. The ecological significance of exchange processes between rivers and groundwater. Freshwater Biology 37:1–33.

Butler, J.J., Jr. 1997. The Design, Performance, and Analysis of Slug Tests. CRC Press LLC, Baca Raton, Florida.

Campbell, G.S., J.D. Jr. Jungbauer, W.R. Bidlake, R.D. Hungerford. 1994. Predicting the effect of temperature on soil thermal conductivity. Soil Science 158:307–313.

Carman, P.C. 1937. Fluid flow through granular beds. Transactions, Institution of Chemical Engineers, London 15:150–166.

Carman, P.C. 1956. Flow of gas through porous media, Butterworths, London.

Carrier, W.D. III., 2003. Goodbye, Hazen; Hello, Kozeny–Carman. Journal of Geotechnical and Geoenvironmental Engineering ASCE 129 (11), 1054–1056, doi:10.1061/(ASCE) 1090–0241(2003)129:11(1054).

Čermák, V., L. Rybach. 1982. Thermal properties. p. 305–343. *In* Angenheister (ed.) Landolt-Börnstein Numerical data and functional relationships in science and technology, Physical properties of rocks, Volume 1a. Springer, New York.

Červený, V., J.E.P. Soares. 1992. Fresnel volume ray tracing. Geophysics 57:902–915.

Chadwick, M.A., J.W. Feminella. 2001. Influence of salinity and temperature on the growth and production of a freshwater mayfly the Lower Mobile River, Alabama. Limnology and Oceanography 46:532–542.

Clark, S.P., Jr. 1966. Thermal conductivity. *In* S.P. Clark, Jr. (ed.) Handbook of physical constants, revised edition, Geological Society of America Memoir 97. GSA, New York.

Cooper, A.J., W.D. Fitzgerald. 1977. Quaternary geology of the Goderich area, Southern Ontario. Ontario Geological Survey Preliminary Map P. 1232.

Cunjak, R.A., G. Power. 1986. Winter habitat utilization by stream resident brook trout (*Salvelinus fontinalis*) and brown trout (*Salmo trutta*). Canadian Journal of Fisheries and Aquatic Science 43:1970–1981.

Curry, R.A., L.G. Noakes, G.E. Morgan. 1995. Ground water and the incubation and emergence of brook trout (*Salvelinus fontinalis*). Canadian Journal of Fisheries and Aquatic Sciences 52:1741–1749.

Curry R.A., D.A. Scruton, K.D. Clarke. 2002. The thermal regimes of brook trout incubation habitats and evidence of changes during forestry operations. Canadian Journal of Forest Research 32:1200–1207, doi:10.1139/X02-046.

de Vries, D.A. 1963. Thermal properties of soils. p. 210–235. *In* W.R. Van Wijk (ed.) Physics of Plant Environment, North-Holland, Amsterdam.

deKozlowski, S.J., D.L. Bunting II. 1981. Laboratory study on the thermal tolerance of four southeastern stream insect species (trichoptera, ephemeroptera). Hydrobiologia 70:141–145.

Desbarats, A.J. 1994. Spatial averaging of hydraulic conductivity under radial flow conditions. Mathematical Geology 26:1–21.

Elliott, J.M., 1994. Quantative Ecology and Brown trout. Oxford University Press: Oxford.

Environment Canada, 2005. Canadian climate normals 1971–2000. website: <http://climate.weatheroffice.ec.gc.ca/climate_normals>.

Feng, S., P.N. Sen. 1985. Geometrical model of conductive and dielectric properties of partially saturated rocks. Journal of Applied Physics 58:3236–3243.

Garside, E.T. 1966. Effects of oxygen in relation to temperature on the development of embryos of brook trout and rainbow trout. Journal of Fisheries Resources Board of Canada 23:1121–1134.

Gaufin, A.R., S. Hern. 1971. Laboratory studies on tolerance of aquatic insects to heated waters. Journal of the Kansas Entomological Society 44:240–245.

Gelhar, L.W. 1993. Stochastic Subsurface Hydrogeology. Englewood Cliffs, New Jersey. Prentice Hall.

Goodrich, L.E. 1982. The influence of snow cover on the ground thermal regime. Canadian Geotechnical Journal 19:421–432.

Hashin, Z., S. Shtrikman. 1962. A variational approach to the theory of the effective magnetic permeability of multiphase materials. Journal of Applied Physics 33: 3125–3131.

Helgeson, H.C., J.M. Delany, H.W. Nesbitt, D.K. Bord. 1978. Summary and critique of the thermodynamic properties of rock-forming minerals. American Journal of Science 278A:1–229.

Hess, K.M., S.H. Wolf, M.A. Celia, S.P. Garabedian. 1991. Macrodispersion and spatial variability of hydraulic conductivity in a sand and gravel aquifer, Cape Cod, Massachusetts. Environmental Research Brief EPA/600//M-91/005, U.S. Environmental Protection Agency, Washington, D.C.

Hess, K.M., S.H. Wolf, M.A. Celia. 1992. Large-scale natural gradient tracer test in sand and gravel, Cape Cod, Massachusetts 3. Hydraulic conductivity variability and calculated macrodispersivities. Water Resources Research 28:2011–2027.

Hogg, I.D., D.D. Williams. 1996. Response of stream invertebrates to a global-warming thermal regime: An ecosystem-level manipulation. Ecology 77:395–407.

Hokanson, K.E.F., J.H. McCormick, B.R. Jones, J.H. Tucker. 1973. Thermal requirements for maturation, spawning, and embryo survival of the brook trout, *Salvelinus fontinalis*. Journal of Fisheries Resources Board of Canada 30:975–984.

Holmes, R.M. 2000. The importance of ground water to stream ecosystem function. p.137–145. *In*: J.B. Jones and P.J. Mulholland (eds.) Groundwater and Streams. Academic Press, San Diego, CA.

Horai, K. 1971. Thermal conductivity of rock-forming minerals. Journal of Geophysical Research 76:1278–1308.

Huisman, J.A., S.S. Hubbard, J.D. Redman, A.P. Annan. 2003. Measuring soil water content with ground-penetrating radar: A review. Vadose Zone Journal 2:476–491.

Hunt, R.J., D.A. Wilcox. 2003. Ecohydrology – why hydrologists should care. Ground Water 41:289.

Hunt, R.J., M. Strand, J.F. Walker. 2006. Measuring groundwater–surface water interaction and its effect

on wetland stream benthic productivity, Trout Lake watershed, northern Wisconsin, USA. Journal of Hydrology, 320, doi:10.1016/j.jhydrol.2005.07.029.

Hynes, H.B.N. 1983. Groundwater and stream ecology. Hydrobiologia 100:93–99.

Ingersoll, l.R., O.J. Zobel, A.C. Ingersoll. 1954. Heat conduction with engineering, geological, and other applications. The University of Wisconsin Press, Madison, Wisconsin, USA, 325 p.

Isard, S.A., R.J. Schaetzl. 1995. Estimating soil temperatures and frost in the lake effect snowbelt region, Michigan, USA. Cold Regions Science and Technology 23:317–332.

Johansen, O. 1975. Thermal conductivity of soils, Ph.D. diss. Trondheim, Norway, (CRREL Draft Translation 637, 1977), ADA 044002.

Kane, D.L., K.M. Hinkel, D.J. Goering, L.D. Hinzman, S.I. Outcalt. 2001. Non-conductive heat transfer associated with frozen soils. Global Planetary Change 29:275–292.

Kluender, R.A., L.C. Thompson, D.M. Steigerwald. 1993. A conceptual model for predicting soil temperatures. Soil Science 156:10–19.

Kozeny, J. 1927. Űberkapillare Leitung des Wassers im Boden: Sitzungsberichte Wiener Akademie, 136:217–306.

Lakly, M.B., J.V. McArthur. 2000. Macroinvertebrate recovery of a post-thermal stream: habitat structure and biotic function. Ecological Engineering 15:S87–S100.

Liberty, B.A., T.E. Bolton. 1971. Paleozoic geology of the Bruce peninsula area, Ontario. Geological Survey of Canada, Memoir 360, 163 p.

Luckner, L., W.M. Schestakow. 1991. Migration proceses in the soil and groundwater zone. Lewis Publishers Inc., Chelsea, Michigan, USA., 485 p.

Lynch, J.A., G.B. Rishel. 1984. Thermal alteration of streams draining clearcut watersheds: quantification and biological implications. Hydrobiologia 111:161–169.

Markle, J.M., R.A. Schincariol, J.H. Sass, J.W. Molson. 2006. The role of thermal conductivity in modeling heat transport through shallow permeable sediments. Soil Science Society of America 70:1281–1294.

Marten, P.S. 1992. Effect of temperature variation on the incubation and development of Brook Trout eggs. The Progressive Fish-Culturist 54:1–6.

McDole, R.E., M.A. Fosberg. 1974. Soil temperatures in selected southeastern Idaho soils: I. Evaluation of sampling techniques and classification of soils. Soil Science Society of America Proceedings 38:480–491.

Mercer, J.W., S.D. Thomas, B. Ross. 1982. Parameters and variables appearing in repository siting models, Report NUREG/CR-3066, U.S. Nuclear Regulatory Commission, Rockville, Maryland, 244 p.

Moench, A.F. 1997. Flow to a well of finite diameter in a homogeneous, anisotropic water table aquifer. Water Resources Research 33:1397–1407.

Moench, A.F. 2004. Importance of the vadose zone in analyses of unconfined aquifer tests. Ground Water

42:223–233.

Molson, J.W., E.O. Frind, C.D. Palmer. 1992. Thermal energy storage in an unconfined aquifer 2. Model development, validation, and application. Water Resources Research 28:2857–2867.

Molz, F.J., J. Guan, J. Wang. 2005. Spatial weighting functions: Transient hydraulic tests and heterogeneous media. Ground Water 43:215–221.

Nebeker, A.V., Lemke, A., 1968. Preliminary studies on the tolerance of aquatic insects to heated waters. Journal of the Kansas Entomological Society 41, 413–418.

Neuman, S.P., 1994. Generalized scaling of permeabilities: Validation and effect of support scale. Geophysical Research Letters 21, 349–352.

Nislow, K.H., Lowe, W.H., 2006. Influences of logging history and riparian forest characteristics on macroinvertebrates and brook trout (*Salvelinus fontinalis*) in headwater streams (New Hapmshire, U.S.A.), Freshwater Biology 51, 388–397, doi:10.1111/j.1365-2427.2005.01492.x.

Noakes, D.L.G., 1989. Early life history and behaviour of charrs. Physiology and Ecology Japan (Spec. Vol.), 1, 173–186.

Oldenborger, G.A., Schincariol, R.A., Mansinha, L., 2003. Radar determination of the spatial structure of hydraulic conductivity. Ground Water 41, 24–32.

Outcalt, S.I., Nelson, F.E., Hinkel, K.H., 1990. The zero-curtain effect: Heat and mass transfer across an isothermal region in freezing soil. Water Resources Research 26, 1509–1516.

Parr, A.D., Molz, F.J., Melville, J.G., 1983. Field determination of aquifer thermal energy storage parameters. Ground Water 21, 22–35.

Power, G., 1980. The brook charr, *Salvelinus fontinalis*. p. 141–203. *In* E.K. Balon (ed.) Charrs. Salmonid fishes of the genus *Salvelinus*, Dr. W. Junk Publishers, The Hague, the Netherlands.

Power, G., Brown, R.S., Imhof, J.G., 1999. Groundwater and fish – insights from northern North America. Hydrological Processes 13, 401–422.

Pugsley, C.W., Hynes, H.B.N., 1986. Three-dimensional distribution of winter stonefly nymphs, *allocapnia pygmaea*, within the substrate of a southern Ontario river. Canadian Journal of Fisheries and Aquatic Sciences 43, 1812–1817.

Quinn, J.M., Steele, G.L., Hickey, C.W., Vickers, M.L., 1994. Upper thermal tolerances of twelve New Zealand stream invertebrates species. New Zealand Journal of Marine and Freshwater Research 28, 391–397.

Rehfeldt, K.R., Boggs, J.M., Gelhar, L.W., 1992. Field study of dispersion in a heterogeneous aquifer 3. Geostatistical analysis of hydraulic conductivity. Water Resources Research 28, 3309–3324.

Rempel, R.S., Carter, J.C.H., 1986. An experimental study on the effect of elevated temperature on the heterotrophic and autotrophic food resources of aquatic insects in a forested stream. Canadian Journal of Zoology 64, 2457–2466.

Reynolds, J.M., 2000. An Introduction to Applied and Environmental Geophysics. Chichester, United Kingdom. John Wiley and Sons. pp. 806.

Robie, R.A., Hemingway, B.S., Fisher, J.R., 1978. Thermodynamic properties of minerals and related substances at 298.15 K and 1 bar (10^5 pascals) pressure and at higher temperatures. U.S. Geological Survey Bulletin 1452, pp.456.

Rovey, C.W., Niemann, W.L., 2001. Wellskins and slug tests: where's the bias? Journal of Hydrology 243, 120–132.

Sánchez-Vila, X., Carrera, J., Girardi, J.P., 1996. Scale effects in transmissivity. Journal of Hydrology 183, 1–22.

Sass, J.H., Lachenbruch, A.H., Munroe, R.J., 1971. Thermal conductivity of rocks from measurements on fragments and its application to heat-flow determinations. Journal of Geophysical Research 76, 3391–3401.

Schmidt, W.L., Gosnold, W.D., Enz, J., 2001. A decade of air-ground temperature exchange from Fargo, North Dakota. Global Planetary Change 29, 311–325.

Schulze-Makuch, D., Carlson, D.A., Cherkauer, D.S., Malik, P., 1999. Scale dependency of hydraulic conductivity in heterogeneous media. Ground Water 37, 904–919.

Schulze-Makuch, D., Cherkauer, D.S., 1998. Variations in hydraulic conductivity with scale of measurement during aquifer tests in heterogeneous, porous carbonate rocks. Hydrogeology Journal 6, 204-215.

Scott, W.B., Crossman, E.J., 1973. Freshwater Fishes of Canada, Fisheries Research Board of Canada Bulletin 184, Ottawa.

Sen, P.N., Scala, C., Cohen, M.H.. 1981. A self-similar model for sedimentary rocks with application to the dielectric constant of fused glass beads. Geophysics 46, 781–795.

Shiozawa, S., Campbell, G.S., 1991. On the calculation of mean particle diameter and standard deviation from sand, silt, and clay fractions. Soil Science 152, 427–431.

Smerdon, J.E., Pollack, H.N., Enz, J.W., Lewis, M.J., 2003. Conduction-dominated heat transport of the annual temperature signal in soil. Journal of Geophysical Research 108 (B9),2431, doi:10.1029/2002JB002351.

Stallman, R.W., 1965. Steady one-dimensional fluid flow in a semi-infinite porous medium with sinusoidal surface temperature. Journal of Geophysical Research 70, 2821–2827.

Taylor, B.R., Dykstra, A.N., 2005. Effects of hot ground water on a small swamp-stream in Nova Scotia, Canada. Hydrobiologia 545, 129–144.

Vannote, R.L., Sweeney, B.W., 1980. Geographic analysis of thermal equilibria: A conceptual model for evaluating the effect of natural and modified thermal regimes on aquatic insect communities, The American Naturalist 115, 667–695.

Williamson, P.R., 1991. A guide to the limits of resolution imposed by scattering in ray tomography. Geophysics 56, 202–207.

Witzel, L.D., MacCrimmon, H.R., 1983. Redd-site selection by brook trout and brown trout in southwestern Ontario streams. Transactions of the American Fisheries Society 112, 760–771.

Wolf, S.H., Celia, M.A., Hess, K.M., 1991. Evaluation of hydraulic conductivities calculated from multiport-permeameter measurements, Ground Water 29, 516–525.

Woodside, W., Messmer, J.H., 1961. Thermal conductivity of porous media. I. Unconsolidated sands. Journal of Applied Physics 32, 1688–1706.

Yang, Zen-Fen, 1995. Application of the Heatflow model in a sand and gravel aquifer. MSc. thesis. Department of Earth Sciences, University of Waterloo, Waterloo, ON.

Zhang, T., Barry, R.G., Gilichinskt, D., Bykhovets, S.S., Sorokovikov, V.A., Jingping Ye, 2001. An amplified signal of climatic change in soil temperatures during the last century at Irkutsk, Russia. Climate Change 49, 41–76.